Experimental and Theoretical Study on the OH-reaction Kinetics and Photochemistry of Acetyl Fluoride (CH₃C(O)F) an Atmospheric Degradation Intermediate of HFC-161 (C₂H₅F)

Xinli Song,[1] Gábor L. Zügner,[2] Mária Farkas,[2] Ádám Illés,[2] Dariusz Sarzyński,[3] Tamás Rozgonyi,[2] Baoshan Wang*[1] and Sándor Dóbé*[2]

[1]College of Chemistry and Molecular Sciences, Wuhan University, Wuhan, 430072, People's Republic of China

[2]Institute of Materials and Environmental Chemistry, Research Centre for Natural Sciences, Hungarian Academy of Sciences, 1117 Budapest, Hungary

[3]Department of Physical Chemistry, Wroclaw Medical University, 50-556 Wroclaw, Poland

ABSTRACT:

The direct reaction kinetic method of low pressure fast discharge flow (DF) with resonance fluorescence monitoring of OH (RF) has been applied to determine rate coefficients for the overall reactions OH + C_2H_5F (EtF) (1) and OH + $CH_3C(O)F$ (AcF) (2). Acetyl fluoride reacts slowly with the hydroxyl radical, the rate coefficient at laboratory temperature is k_2 (300 K) = (0.74 ± 0.05) × 10^{-14} cm^3 $molecule^{-1}$ s^{-1} (given with 2σ statistical uncertainty). The temperature dependence of the reaction does not obey the Arrhenius law and it is described well by the two-exponential rate expression of k_2 (300–410 K) = 3.60 × 10^{-3} exp(–10500 / T) + 1.56 × 10^{-13} exp(–910 / T) cm^3 $molecule^{-1}$ s^{-1}. The rate coefficient of k_1 = (1.90 ± 0.19) × 10^{-13} cm^3 $molecule^{-1}$ s^{-1} has been determined for the EtF-reaction at room temperature (T = 298 K).

Microscopic mechanisms for the OH + $CH_3C(O)F$ reaction have also been studied theoretically using the ab initio CBS-QB3 an G4 methods. Variational transition state theory was employed to obtain rate coefficients for the OH + $CH_3C(O)F$ reaction as a function of temperature on the basis of the ab initio data. The calculated rate coefficients are in good agreement with the experimental data. It is revealed that the reaction takes place predominantly via the indirect H-abstraction mechanism involving H-bonded prereactive complexes and forming the nascent products of H_2O and the CH_2CFO radical. The non-Arrhenius behavior of the rate coefficient at temperatures below 500 K is ascribed to the significant tunneling effect of the in-the-plane H-abstraction dynamic bottleneck. The production of FC(O)OH + CH_3 via the addition/elimination mechanism is hardly competitive due to the significant barriers along the reaction routes.

Photochemical experiments of AcF were performed at 248 nm by using exciplex lasers. The total photodissociation quantum yield for $CH_3C(O)F$ has been found significantly less than unity; among the primary photochemical processes, C–C bond cleavage is by far dominating compared with CO-elimination. The absorption spectrum of AcF has also been determined displaying a strong blue shift compared with the spectra of aliphatic carbonyls.
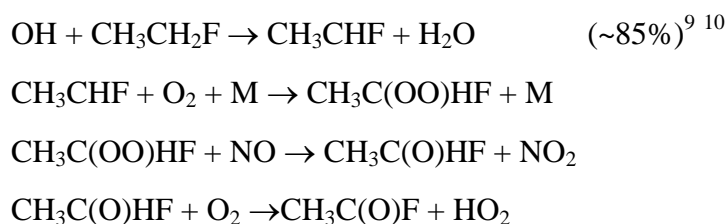
Consequences of the results on atmospheric chemistry have been discussed.

1. INTRODUCTION

The consumption and global emissions of hydrofluorocarbons (HFCs), used predominantly for refrigeration and air conditioning (AC), are forecasted to increase very substantially the coming decades[1][2]. These substances do not destroy the Earth's protecting ozone layer, but most of them are potent greenhouse gases (GHGs) which have high global warming potential (GWP) and are projected to amount to 9–19% of the climate forcing of CO_2 by the year 2050[1,2]. It is understood then that there are more and more stringent regulations and initiatives[3][4] to phase out / phase down the production and use of high GWP HFCs and to secure low GWP substitutes and alternatives.

A new, promising refrigerant is C_2H_5F (HFC-161). Its 100-year GWP is 4[5], which is much smaller than the same metrics of other HFCs currently in use[5]. As for instance, CF_3CH_2F (HFC-134a), which is still the most widely applied HFC in AC systems, has a 100-year GWP of 1300[5]. HFC-161 has excellent refrigeration properties with high coefficient of performance (COP), but its flammability is a disadvantage, thus it will likely be used blended with other HFCs. [6][7][8]

Beyond low GWP, a good substitute needs to meet several other requirements as well, including that its atmospheric degradation products should also be climate friendly and must not lead to the deterioration of air quality. By analogy with other HFCs and hydrocarbons, C_2H_5F (EtF) is likely to undergo the following oxidation steps under tropospheric conditions:

$$OH + CH_3CH_2F \rightarrow CH_3CHF + H_2O \qquad (\sim 85\%)^{9\ 10}$$
$$CH_3CHF + O_2 + M \rightarrow CH_3C(OO)HF + M$$
$$CH_3C(OO)HF + NO \rightarrow CH_3C(O)HF + NO_2$$
$$CH_3C(O)HF + O_2 \rightarrow CH_3C(O)F + HO_2$$

That is, the atmospheric depletion of C_2H_5F is initiated by the reaction with OH, H-abstraction occurs predominantly from the α-position of the molecule at room temperature[9][10] and acetyl fluoride ($CH_3C(O)F$, AcF) is expected to be formed as a major reaction intermediate in the OH-initiated photo-oxidation. In a recent smog chamber study[11], AcF has been observed with a high yield during the photo-degradation of CH_3CHF_2 (HFC-125a) at high NOx concentrations. HFC-125a has a relatively small GWP (138 at the 100 years time horizon[5]) and its atmospheric abundance is increasing rapidly[2][12].

The atmospheric fate of acetyl fluoride is determined potentially by its reaction with OH, photolysis and wash-out; practically no information is available on either of these

processes from experiment or theory. Here we report results mostly on the OH + CH$_3$C(O)F reaction and photolysis of AcF with the motivation of gaining new knowledge on the effect of fluorine substitution on the reactivity and photochemistry of an aliphatic carbonyl molecule and provide data and mechanistic information for modeling atmospheric chemistry and combustion. Focus of our research has been the experimental and theoretical study of the kinetics and mechanism of the reaction of OH with acetyl fluoride.

Unlike acetyl fluoride, the elementary reaction of *acetone* with OH radical has been the subject of numerous experimental (see, e.g., refs. [13] [14] [15, 16] [17] [18] [19] [20] [21]) and theoretical (see, e.g., refs. [14] [17] [19] [20] [22] [23] [24] [25]) investigations. Hence, OH + CH$_3$C(O)CH$_3$ has become one of the best known of all OH reactions providing the opportunity to assess the effect of F-substitution on the reactivity by comparison with our results of the OH + CH$_3$C(O)F reaction. The rate coefficient of the overall reaction at room temperature is k(OH + acetone, 298 K) = 1.8×10^{-13} cm^3 molecule^{-1} s^{-1} (with ~5% maximal uncertainty), the temperature dependence of the reaction deviates from the Arrhenius law, the reaction takes place via hydrogen abstraction, addition of OH to the >C=O bond and subsequent elimination reaction of the adduct is much less important.[26] Theoretical studies have revealed the molecular mechanisms of the hydrogen abstraction reaction route to form H$_2$O + CH$_3$C(O)CH$_2$ and the addition/elimination reaction route to form CH$_3$ + CH$_3$C(O)OH. Both mechanisms involve weakly bonded "prereactive" (or "prereaction") van der Waals complexes formed on along the reaction path via intermolecular hydrogen bonding. The loose complexes have just a few kcal/mol stabilization energy, yet have profound effect on the kinetics of the reaction, most prominently by increasing the quantum chemical tunnel effect for hydrogen abstraction reactions.

We have performed direct kinetic experiments to determine rate coefficients, k_1 and k_2, for the overall reactions of OH with C$_2$H$_5$F and CH$_3$C(O)F; the ethyl fluoride reaction served essentially as a test case, since its rate coefficient is well known [26].

$$\text{OH} + \text{C}_2\text{H}_5\text{F} \rightarrow \text{products} \qquad\qquad (1)$$

$$\text{OH} + \text{CH}_3\text{C(O)F} \rightarrow \text{products} \qquad\qquad (2)$$

In the photochemistry experiments of AcF, the total (consumption) quantum yield, Φ_3, and the primary quantum yields, φ_{3a} and φ_{3b}, have been determined at 248 nm photolysis wavelength. The absorption cross section as a function of wavelength, $\sigma_{\text{AcF}}(\lambda, 298 \text{ K})$, has also been determined.

$$CH_3C(O)F + h\nu \rightarrow products \tag{3}$$

$$\rightarrow CH_3 + C(O)F \tag{3a}$$

$$\rightarrow CH_3F + CO \tag{3b}$$

The energetic profiles of the OH + $CH_3C(O)F$ reaction system has been mapped in great details by using high level quantum chemistry methods, and the ab initio data obtained for the lowest-energy reaction pathways have been utilized in theoretical reaction kinetic computations within a variational transition state theory (VTST) framework.

2. EXPERIMENTAL METHODS

2.1 Discharge Flow Technique

The low pressure fast discharge flow method (DF) coupled with resonance fluorescence detection of OH radicals (RF) was applied to study the kinetics of the reactions of OH with C_2H_5F and $CH_3C(O)F$. The apparatus and experimental procedure have been described in detail previously [27,28] and so only a brief summary is presented here.

The experiments were performed in a jacketed Pyrex reactor which had an internal diameter of 4.0 cm and total length of 64 cm. The inner surface of the reactor was coated with a thin layer of halocarbon wax (HCW) to minimize the heterogeneous loss of OH radicals. The reaction temperature was varied by circulating thermostating liquid through the jacket of the flow tube providing a reaction zone of 45 cm with constant temperature at ± 1 K (errors throughout the paper refer to 2σ, precision only). The reaction temperature was measured inside the reactor by using a retractable thermocouple. Helium was the carrier gas. The reactor was equipped with a movable injector to vary the reaction time (distance). OH radicals were produced by the fast reaction H + $NO_2 \rightarrow$ OH + NO inside the injector and H-atoms were obtained by microwave dissociation of H_2 in He flow. The reaction pressure was measured with a capacitance manometer.

The flow reactor was connected downstream to a detection cell to monitor OH. The OH(A–X) excitation radiation was provided by a microwave-powered resonance lamp operated with water-saturated Ar flow at ~2 mbar pressure. The induced fluorescence emanating from the detection volume was passed through an interference filter ($\lambda_{max} = 310$ nm) and detected by a photomultiplier (PM). The analogue signal from the PM was fed into a purpose-built hardware-software unit which provided online estimation of rate coefficients

from the experiments. The minimum detectable OH concentration was ~2×10^9 molecules cm^{-3}.

2.2 Measurements of Absorption Cross Sections

The UV absorption spectrum of acetyl fluoride was determined employing a home-constructed gas spectrophotometer[28, 29]. The analysis light was provided by a D$_2$ lamp, the collimated light beam of which was passed through a thermostated absorption cell, then dispersed spectrally by a monochromator and detected by a photomultiplier (PM). The PM was interfaced to a digital control and data acquisition system to provide automatic recording of spectra. The spectral resolution was ~0.4 nm.

2.3 Laser Photolysis Technique

Exciplex laser photolysis (PLP) at 248 nm was applied to determine total photodissociation quantum yields and product quantum yields (QYs) by measuring, respectively, the concentration depletion of acetyl fluoride and the formation of stable photolysis products by using GC analysis. The experimental methodology is similar to that applied by Gierczak et al.[30] and is described in detail in our previous publication[29]. Photolysis experiments were carried out in a 20.0 (optical path) × 2.3 cm (internal diameter) cylindrical fused silica cell. The cell was equipped with a septum joint to withdraw samples for GC analysis. The analysis was performed on a 30 m HP-5 quartz capillary column at 303 K using flame-ionization detection. Most of the photolysis experiments were carried out in synthetic air buffer gas and the reaction mixture usually contained 1,1,2,2-tetrafluoroethane (TFE) as an internal GC standard. The input laser energy was measured with a calibrated laser energy meter, the energy was typically ~40 mJ pulse^{-1} and the laser was operated at 5 Hz.

2.5 Materials.

Acetyl fluoride reacts very slowly with OH, so it was crucial to use high purity chemicals in the experiments. CH$_3$C(O)F was purchased from PCR Inc. (>96% purity) and also from abcr GmbH&Co (99.5% purity). No contamination could be found in either sample by GC analysis performed on two different polarity columns. Most of the experiments were conducted with the PCR acetyl fluoride, but tests with samples from the other supplier have shown no systematic variation of the kinetic results. Acetyl fluoride is prone to hydrolysis, it reacts even with the moisture of glass surfaces at standing. No indication for hydrolysis and

well-reproducible results were obtained, however, when AcF was metered into the reactors directly from the metal containers (kept at melting ice slurry). *Ethyl fluoride* (SynQuest Lab. Inc., >97%) was used as provided.

The GC standard 1,1,2,2-tetrafluoroethane (PCR Inc., >99%) was degassed by freeze–pump-thaw cycles prior to use. The suppliers and purity of the gases used were as follows: He (Messer-Griesheim, 99.996%), H_2 (Linde Gas, 99.98%), Ar (Linde Gas, 99.999%), synthetic air (Messer-Hungaria, >99.5%). NO_2 (Messer-Griesheim, 98%) was purified by repeated low-temperature trap-to-trap distillations in vacuum.

3. EXPERIMENTAL RESULTS AND DISCUSSION

3.1 DF-RF Determination of Rate Coefficients

Rate coefficients, k_1 and k_2, respectively for the overall reactions (1) and (2) were determined under pseudo-first order conditions with high excess of the reactants over the initial OH concentration, that is, $[C_2H_5F]$, $[CH_3C(O)F] \gg [OH]_0 \approx 2 \times 10^{11}$ molecule cm^{-3}.

$$OH + C_2H_5F \rightarrow products \qquad (1)$$
$$OH + CH_3C(O)F \rightarrow products \qquad (2)$$

The experiments were performed by recording the OH resonance fluorescence signal amplitudes vs. the varied reaction distance, Δz, with, S^{OH}_{on}, and without, S^{OH}_{off}, of the reactants' flows ("on-off" measurement technique [31]). Under the plug-flow condition of the experiments, the reaction time equals $(\Delta z / v_{lin})$, where v_{lin} is the average linear flow velocity in the flow tube. Assuming first-order kinetics and with the provision that the wall activity for OH is not very different in the presence and absence of the reactants, the experimental data were evaluated by using eqs I–III:

$$-\ln (S^{OH}_{on} / S^{OH}_{off}) = k_{i\square}' (\Delta z / v_{lin}) \qquad (I)$$
$$k_{i\square}' = k_{i\square} [R(i)] + const \qquad (II)$$
$$-\ln S^{OH}_{off} = k_w (\Delta z / v_{lin}) \qquad (III)$$

where $k_{i\square}'$ is the pseudo-first order rate coefficient (decay constant), $i = 1$ and 2, R(1) = C_2H_5F and R(2) = $CH_3C(O)F$ (2), k_w designate the rate coefficient of the depletion of OH on the walls of the reactor.

3.2 Kinetic Studies of Ethyl Fluoride Reactions

3.2.1 Rate Coefficient for OH + C$_2$H$_5$F (1)

k_1 has been determined at room temperature. Plots of the experimental data according to eqs (I)–(III) have been presented in Figure 1: the inset shows selected OH decays in semi-logarithmic representation, and the main panel of the figure shows the plot of pseudo-first order rate coefficients vs. the ethyl fluoride concentration. The k_1 and k_1' rate coefficients have been obtained by linear least-squares analyses (LSQ). The experimental conditions and kinetic results are summarized in Table 1. In the current work, we have not corrected the measured pseudo-first order rate coefficients for viscous flow and axial diffusion: our previous experience and reports from other laboratories[32] suggest such corrections to be less than ~5%. The proposed rate coefficient for the overall reaction of OH with C$_2$H$_5$F is the following:

$$k_1(298 \text{ K}) = (1.90 \pm 0.19) \times 10^{-13} \text{ cm}^3 \text{ molecule}^{-1} \text{ s}^{-1}$$

This value agrees reasonable well with the rate coefficient of $k_1(298 \text{ K}) = 2.2 \times 10^{-13}$ cm^3 molecule^{-1} s^{-1} recommended (with ~15% uncertainty) by the most recent NASA-JPL critical data evaluation[26]. While all previous kinetic measurements involved photolytic generation of OH radicals, the rate coefficient we report here has been determined by using the thermal DF technique. The possible systematic errors are different with the two methods and so the agreement mutually confirms the reliability of the kinetic data. The OH + C$_2$H$_5$F reaction has also served to test the new data acquisition and analysis system of our experiments.

3.2.2 Photo-oxidation of Ethyl Fluoride

In order to assess the atmospheric fate of ethyl fluoride, a few OH-initiated photo-oxidation experiments were performed in a 10 L Pyrex-bulb photo-reactor in 1 bar synthetic air. OH radicals were produced by the photo-oxidation of CH$_3$ONO and irradiations were accomplished by the filtered light ($\lambda_{max} = 362$ nm) of a high power Xe lamp (for technical details see ref [33]).

The consumption of EtF and the formation of products as a function of irradiation time were followed by GC analysis (using Rt-QS-Bond column). Acetyl fluoride has been unequivocally identified among the reaction products; its time history revealed build-up concomitant with the depletion of ethyl fluoride and was the major product in two

experiments of three. No quantitative AcF yield could be determined, however, because of the large scatter of the data. Nevertheless, these qualitative results are in accordance with the expectations based on similar reaction systems (see also in the Introduction).

Table 1. Experimental Conditions and Kinetic Results for the Reactions of OH Radicals with Ethyl Fluoride and Acetyl Fluoride Using the DF-RF Experimental Method [a]

T (K)	p (mbar)	[EtF] (10^{13} molecules cm^{-3})	v_{lin} (cm s^{-1})	k'_1 (s^{-1})	k_w (s^{-1})	k_1 (10^{-13} cm^3 molecule^{-1} s^{-1})	No. of expts
Reaction OH + C$_2$H$_5$F → products (1)							
298 ± 2	2.60	3.0–18.6	398–539	8.6–36.7	6.0–15.0	1.90 ± 0.19	14

T (K)	p (mbar)	[AcF] (10^{14} molecules cm^{-3})	v_{lin} (cm s^{-1})	k'_2 (s^{-1})	k_w (s^{-1})	k_2 (10^{-14} cm^3 molecule^{-1} s^{-1})	No. of expts
Reaction OH + CH$_3$C(O)F → products (2)							
300 ± 2	2.37	2.7–26.5	361–437	9.0–29.5	5.5–18.2	0.74 ± 0.10	21
342 ± 1	2.50	6.9–63.0	690–839	4.1–70.5	1.3–6.0	1.08 ± 0.06	14
371 ± 1	2.59	2.2–23.1	755–844	6.9–39.0	2.8–30.3	1.55 ± 0.14	13
390 ± 1	2.61	3.7–23.1	879–1033	9.7–53.2	1.7–19.5	2.17 ± 0.38	16
410 ± 2	2.50	3.6–35.6	883–1027	11.3–95.9	1.8–17.3	4.60 ± 0.24	10

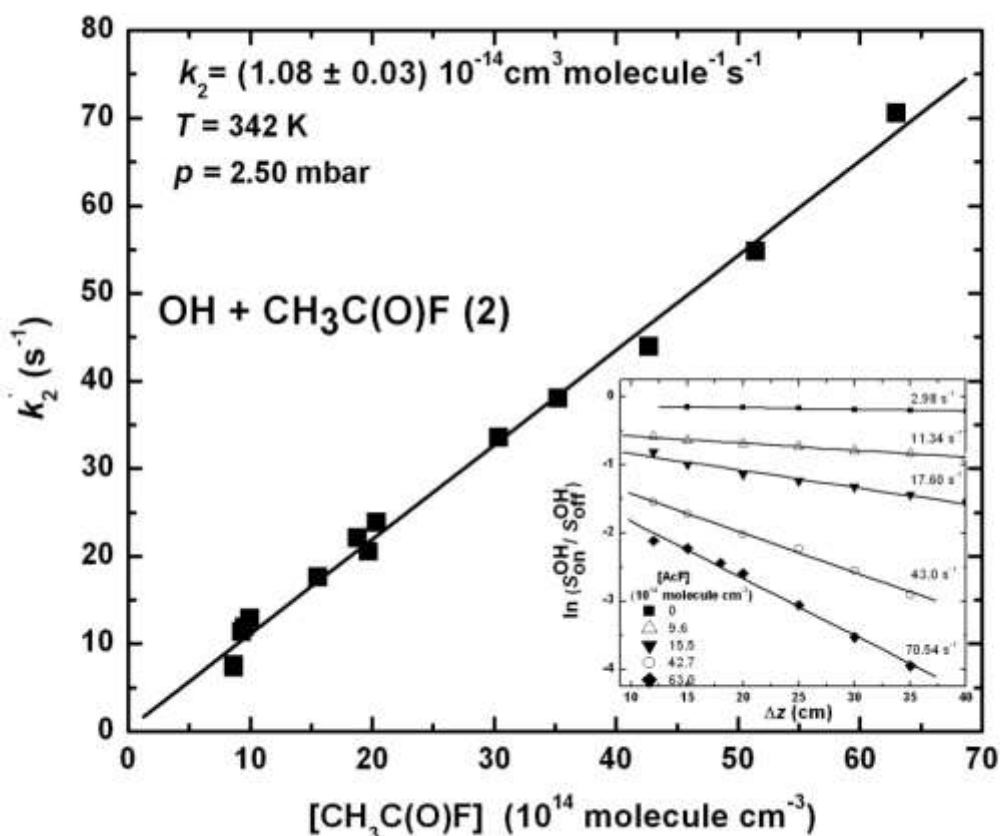[a] The errors represent 2σ statistical uncertainties.
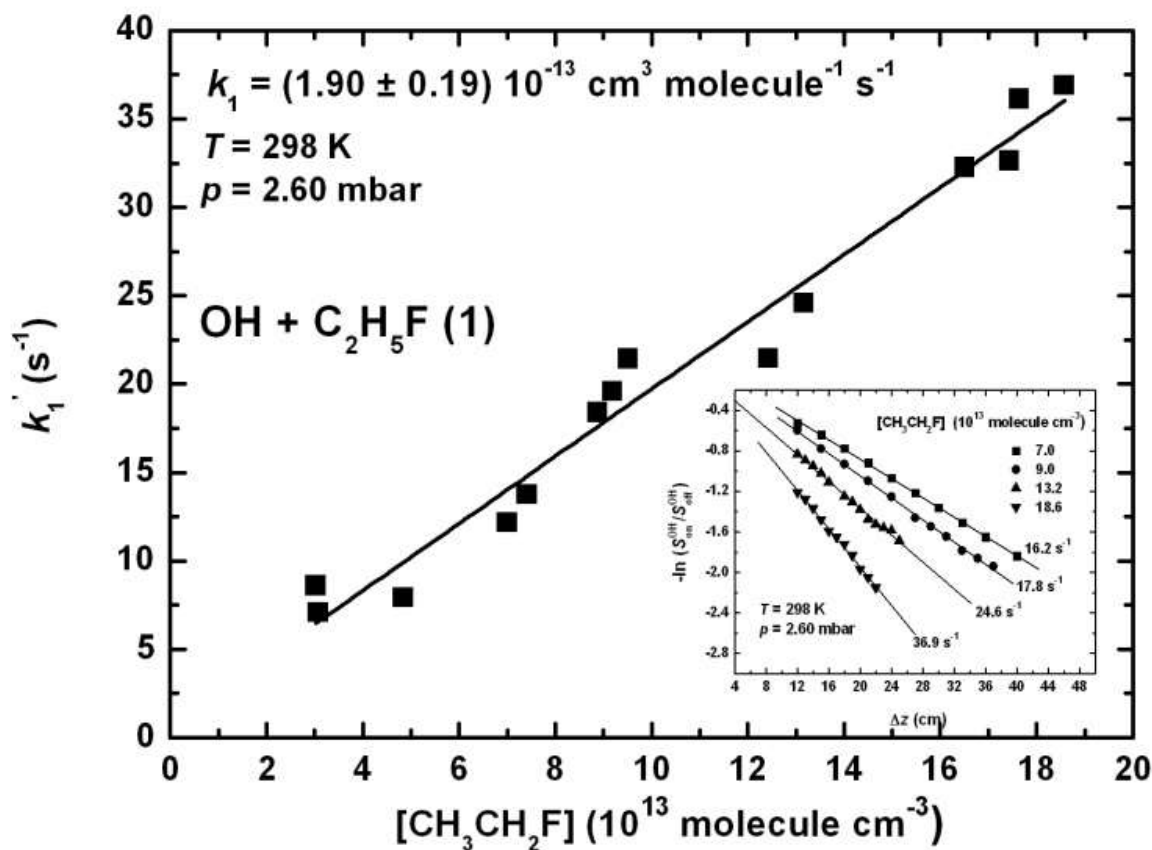
Figure 1. Pseudo-first order plots used for the determination of rate coefficient for the overall reaction of OH with C_2H_5F at $T = 298$ K and $p = 2.60$ mbar He pressure.

3.3 Kinetics of the Reaction of OH Radical with Acetyl Fluoride

Rate coefficients for the overall reaction OH + $CH_3C(O)F$ (2) have been determined at five temperatures over the temperature range of $T = 300–410$ K at $p \approx 2.5$ mbar He pressure.

k_2 values were determined from pseudo-first order experiments and evaluation procedure as outlined in Section 3.1. Representative pseudo-first order OH decays at 342 K are presented as semi-logarithmic plots in the inset of Figure 2 and k'_2 vs. acetyl fluoride concentration data are plotted for the same temperature in the main panel. The linearity of the pseudo-first order plots indicate that reaction (2) was studied under kinetically isolated conditions; k'_2 and k_2 have been obtained as LSQ slopes. Because of the low reactivity of OH with $CH_3C(O)F$, the measured pseudo-first order rate coefficients are small values, but display relatively little scatter. This can be attributed to the application of the "AcF on" –

"AcF off" measurement protocol that can significantly reduce the effects of the fluctuation or drift of experimental conditions (initial OH concentration, intensity of the RF lamp, reaction pressure, etc.)[31]. Pseudo-first order kinetics were obeyed well at the other temperatures too; the respective plots are presented as Supporting Information (SI) (Figs. SI-1–SI-4 in SI). The ln S^{OH}_{off} data when plotted against the reaction time gave also straight lines, their slopes provided $k_w \approx 10$ s^{-1} rate coefficient for the heterogeneous loss of OH independent of temperature. This "wall rate coefficient" is of the usual magnitude or even smaller than we had experienced previously at DF studies of other OH reactions using HCW wall coating. Reaction conditions used and kinetic results obtained in the study of the OH + CH$_3$C(O)F (2) reaction are summarized in the second part of Table 1.

Figure 2. Pseudo-first order plots used for the determination of rate coefficient for the overall reaction of OH with CH$_3$C(O)F at $T = 342$ K and $p = 2.50$ mbar He pressure.

To the best of our knowledge, no kinetic data for the reaction of OH with CH$_3$C(O)F have been reported. k_2 is a very small value, as it is seen, for example, by comparison with the room temperature rate coefficients of a few related OH reactions (given in 10^{-15}

molecule^{-1} cm^3 s^{-1} and taken from ref.[26] and our current work): k (OH + C$_2$H$_6$) = 8700, k_1 (OH + C$_2$H$_5$F) = 190, k (OH + CH$_3$C(O)CH$_3$) = 180 and k_2 (OH + CH$_3$C(O)F) = 7.36. This trend is understood, by the combined strong negative inductive effects of the F-atom and C=O group in determining the reactivity of the electrophilic OH radical with the CH$_3$C(O)F molecule. Based on the measured rate coefficient, the F(FCO) = 0.054 group-reactivity factor is proposed (T = 298 K) that can be used for the estimation of rate coefficients for other OH + acyl-fluoride reactions by using Atkinson's structure–activity (SAR) method [34].
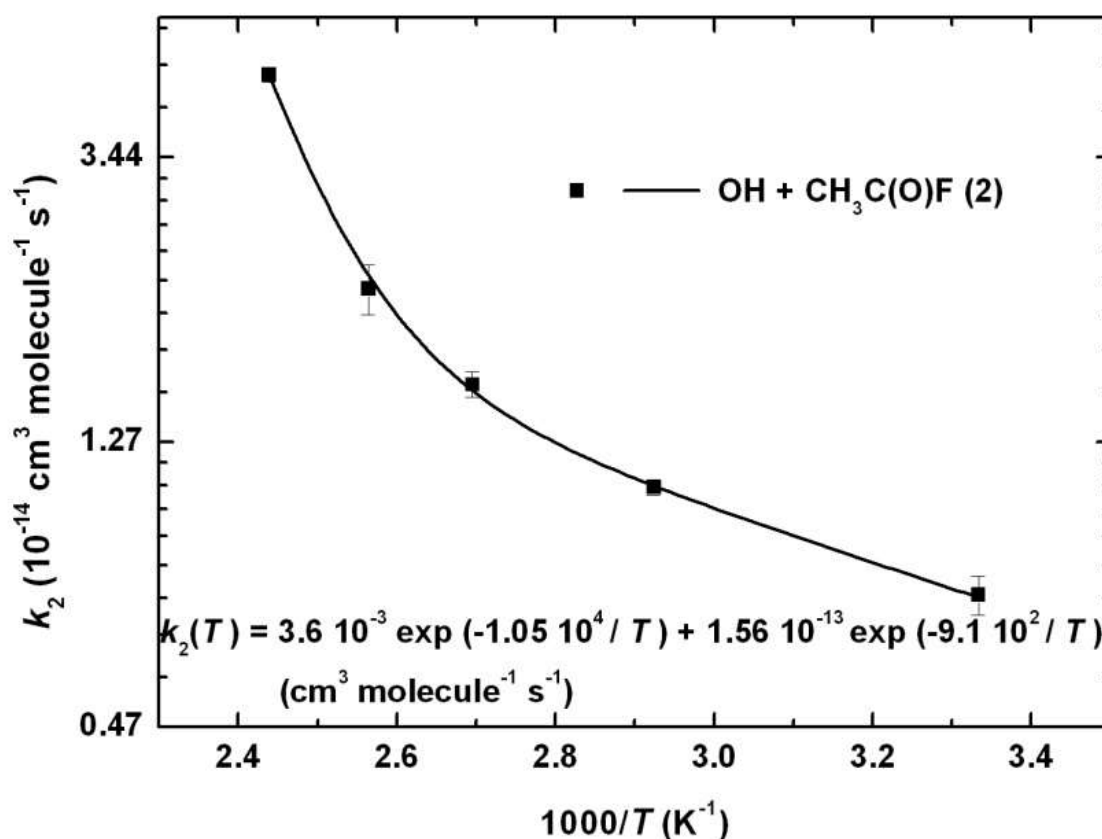
Figure 3. Arrhenius plot for the reaction of OH with acetyl fluoride. The solid line is a fit of a double-exponential expression to the experimental data.

The experimentally determined rate coefficients are plotted on a logarithmic scale versus (1 / T) in Figure 3; the Arrhenius plot is seen to deviate very significantly from linearity displaying an upward curvature towards higher temperatures. A double-exponential function has been fitted to the experimental data by using weighted, non-linear least-squares procedure which has returned,

$$k_2(300\text{–}410 \text{ K}) = 3.60 \times 10^{-3} \exp(-10500 / T) + 1.56 \times 10^{-13} \exp(-910 / T) \text{ cm}^3 \text{ molecule}^{-1} \text{ s}^{-1}$$

$$\text{(IV)}$$

The average deviation of this proposed rate coefficient expression from the experimental data is less than 2%. Equation (IV) is a convenient representation of the temperature dependence of the reaction of OH with AcF, but within the studied temperature range only, and the given constants should be considered merely as empirical parameters of the fit without having real physical meaning.

The curvature of the Arrhenius plot has been well documented to occur for numerous elementary reactions of OH radical [26, 35]. A modified, three-parameter Arrhenius expression is frequently used to describe the temperature dependence for reactions with smaller deviation from linearity, such as the reactions of OH with HFCs[36] and fluoro alcohols [37]. The Arrhenius plots of some of the reactions of OH with carbonyl molecules exhibit stronger curvature, such as OH + acetone[13 15] and OH + acetic acid[38], the temperature dependences of which have been recommended to be given in the form of a double exponential function similar to equation (IV). The three-parameter Arrhenius function has provided a slightly less satisfactory fit to the experimental data of the OH + acetyl fluoride reaction compared with equation (IV) [28].

In passing we note that in most of the OH kinetic experiments, including our present one, the rate coefficient for the overall reaction is determined while the reason of non-Arrhenius behavior is connected to mechanistic features of the related elementary reactions that can be revealed by high-level quantum chemical and theoretical reaction kinetic computations. Conversely, high precision experimental kinetic data provide rigorous tests for assessing the performance of the different theoretical methods.

3.4 Photochemistry of Acetyl Fluoride

3.4.1 The Absorption Spectrum of Acetyl Fluoride

The gas phase absorption spectrum for $CH_3C(O)F$ was measured over the wavelength range of $\lambda = 200\text{–}300$ nm, at room temperature ($T = 298 \pm 1$ K). The wavelength-dependent cross-sections, $\sigma_{AcF}(\lambda)$, were obtained from absorption measurements applying the Beer–Lambert law:

$$A = \ln \{(I_0) / (I)\} = \sigma_{AcF}(\lambda) L [\text{AcF}] \qquad \text{(V)}$$

where A is the measured absorbance, L (= 50.2 cm, or 11.6 cm) is the optical path length and I_0 and I are the transmitted light intensities in the absence and in the presence of acetyl fluoride, respectively.

The Beer–Lambert (BL) plots of A versus [AcF] provided straight lines, but had substantial intercepts below ~215 nm wavelength at higher concentrations (see Figure SI-5 in the Supporting Information). Therefore, the absorption cross sections were determined at each wavelength in concentration ranges where the BL lines had zero intercepts using linear LSQ procedure. The positive intercepts may be due to adsorption of $CH_3C(O)F$ on the windows of the absorption cell.

The absorption spectrum is shown in Figure 4 and the corresponding absorption cross sections, $\sigma_{AcF}(\lambda)$, are tabulated in 1 nm intervals in the Supporting Information (Table SI-1). Most of the measurements were carried out with our gas spectrophotometer, but the absorption cross section at 248 nm was determined also by using a reduced intensity KrF laser as the analytical light source. The combined data set of the two series of measurements is presented as a common BL plot in the inset of Figure 4 providing: σ_{AcF}(248 nm, 298 K) = $(2.03 \pm 0.08) \times 10^{-21}$ cm^2 molecule^{-1}. This absorption cross section value has been utilized for calculating the photolysis QY of acetyl fluoride (Section 3.4.2).

The absorption spectrum of acetyl fluoride has a wide absorption band with a maximum at ~208 nm extending to ~260 nm at longer wavelengths. By analogy with aliphatic aldehydes and ketones, the absorption band is believed to correspond to an n→π* electronic transition of the C=O group from the ground state to the first electronically excited singlet state. The electron withdrawing F-substituent attached to the C=O group shifts the absorption spectrum strongly, by ~70 nm in the "blue" direction compared, for example, with acetaldehyde and acetone.

The absorption spectrum of AcF has been measured by Rattigan and co-workers[39] using a dual-beam spectrophotometer; their spectrum is also depicted in Figure 4 for comparison. The two spectra are seen to agree well, the average absolute deviation is less than 4% between 200 and 260 nm. Rattigan et al. have reported a second, week absorption band above 260 nm as well that we could not detect probably because of the lower sensitivity of our apparatus.
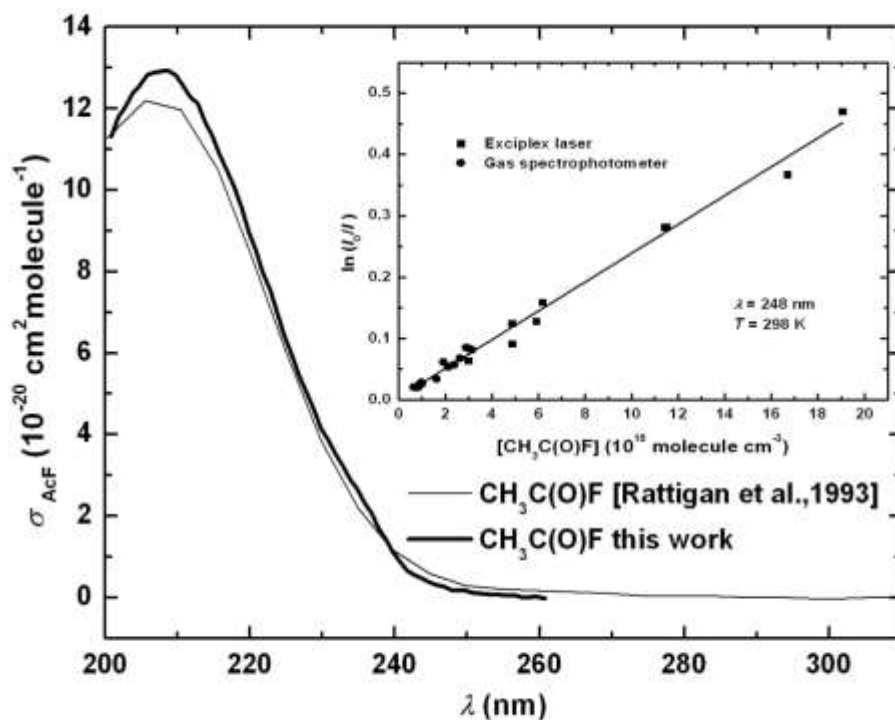
Figure 4. The absorption spectrum of acetyl fluoride (T = 298 K). The Beer-Lambert plot in the inset shows the determination of the absorption cross section at 248 nm using a spectrophotometer and also a reduced intensity exciplex laser as the analytical light source. The thin line displays the spectrum reported in ref [39].

3.4.2 Photodissociation Quantum Yield of Acetyl Fluoride

The total photodissociation quantum yield of acetyl fluoride, Φ_3(248 nm), was determined at room temperature (T = 298 ± 2 K) in synthetic air at 1 bar total pressure. The O_2 content of the synthetic air converted the free radical products to unreactive peroxy radicals precluding also their recombination back to the acetyl fluoride molecule.

$$CH_3C(O)F + h\,v \rightarrow products \tag{3}$$

The concentration of AcF was measured before photolysis, $[AcF]_0$, and after n laser shots, $[AcF]_n$ by GC analysis; fresh gas mixtures were prepared for each irradiation. The experimental data were evaluated according to eq (VI) [28,29, 30]

$$\ln ([\text{AcF}]_n / [\text{AcF}]_0) = - C \times \Phi_3(248 \text{ nm}) \times (n \times E) \tag{VI}$$

$$\text{with } C = f_w(248 \text{ nm}) \times E_{Ph}(248 \text{ nm})^{-1} \times \sigma_{AcF}(248 \text{ nm}) \times L \times V^{-1}$$

where E is the laser energy (mJ) per pulse $f_w(248 \text{ nm})$ is the transmission of the entrance window (the measured value was 0.885 for one window), $E_{Ph}(248 \text{ nm})$ is the energy of one photon (mJ photon^{-1}), L (= 20.0 cm) is the optical path length, and V is the total volume of the cell (cm^3). $\Phi_3(248 \text{ nm})$ was obtained by plotting $\ln ([\text{AcF}]_n / [\text{AcF}]_0)$ against $(n \times E)$ and making use of the absorption cross section measured in the current work and the known parameters in eq. (VI). The initial concentration was $[\text{AcF}]_0 \approx 3.2 \times 10^{17}$ molecules cm^{-3} (~13 mbar) and the consumption of $CH_3C(O)F$ was in the range of 5–30 %.

A plot of $\ln ([\text{AcF}]_n / [\text{AcF}]_0)$ versus $(n \times E)$ is presented in Figure 5. The plotted data determine straight line although with quite substantial scatter. The reason of the data scatter is unclear, since the photolysis mixture contained TFE as an inert GC internal standard to facilitate precise determination of the concentrations. Linear least squares analysis has provided the following result for the overall QY of the photolysis of acetyl fluoride:

$$\Phi_3(248 \text{ nm}, 298 \text{ K}) = 0.62 \pm 0.05$$
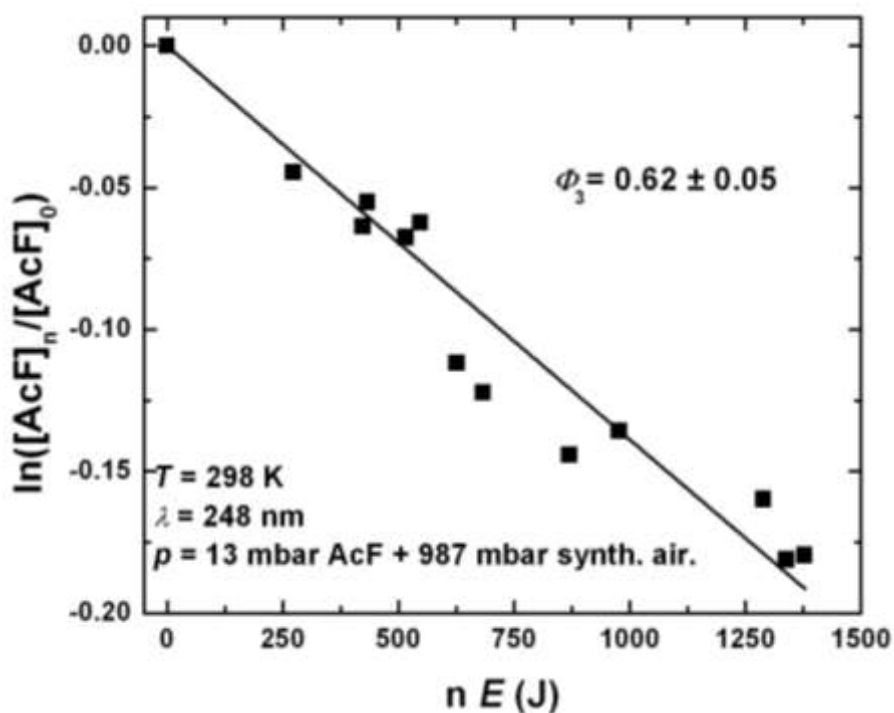
Figure 5. Plot used to determine the photodissociation quantum yield of acetyl fluoride: $[\text{AcF}]_n$ and $[\text{AcF}]_0$ designate the measured concentration at a given reaction time and at time zero, respectively, n is the number of laser pulses and E(J) is the energy per pulse.
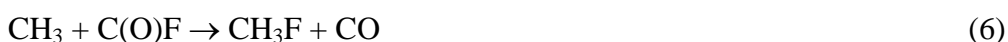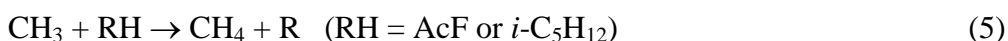
3.4.3 Photolysis Products and Mechanism

Survey experiments were performed to assess the formation of products in the 248 nm photolysis of acetyl fluoride by irradiating pure acetyl fluoride samples, mixtures of $CH_3C(O)F$ with i-pentane an H-donor additive, and O_2 a free radical chaperon. Flame ionization detection of our GC made possible the measurement of the photolysis products of CH_4, CH_3F and C_2H_6. The experiments were conducted at low conversion of $CH_3C(O)F$, below ~3%, when the product quantum yields, $\Phi_{PP}(248\ K)$, could be estimated by the expression:

$$\Phi_{PP}(248\ K) = [PP]_n / \{C \times [AcF]_0 \times (n \times E)\} \qquad (VII)$$

where $[PP]_n$ designate concentrations of the photolysis products, CH_4, CH_3F and C_2H_6, after irradiating the samples by n laser pulses and C is the same constant as in eq. (VI).

The product quantum yields have been summarized in Table 2. The QYs determined in the presence and absence of additives are in accordance with a mechanism comprising the following primary (3a)–(3b) and secondary (4)–(10) photochemical processes:

$$CH_3C(O)F + h\,v \rightarrow CH_3 + C(O)F \qquad (3a)$$
$$\rightarrow CH_3F + CO \qquad (3b)$$

$$CH_3 + CH_3 + M \rightarrow C_2H_6 + M \qquad (4)$$
$$CH_3 + RH \rightarrow CH_4 + R \quad (RH = AcF\ or\ i\text{-}C_5H_{12}) \qquad (5)$$
$$CH_3 + C(O)F \rightarrow CH_3F + CO \qquad (6)$$
$$CH_3 + C(O)F + M \rightarrow CH_3C(O)F + M \qquad (7)$$
$$CH_3 + O_2 \rightarrow products \qquad (8)$$
$$FCO + O_2 \rightarrow products \qquad (9)$$
$$R + O_2 \rightarrow products \qquad (10)$$

According to the proposed mechanism, the sum of the product quantum yields provides approximately the total photodissociation QY as $\Phi_\Sigma = \Phi_{CH4} + 2\Phi_{C2H6} + \Phi_{CH3F} \approx \Phi_3$ in the range of 0.6–0.7 (Table 2) in line with the $\Phi_3 = 0.62$ value determined by measuring the photolytic loss of AcF. Addition of O_2 almost completely quenches the formation of methyl fluoride, the observed small yield gives an upper limit for the quantum yield of the primary process of molecular elimination: $\varphi_{3b} \leq \Phi_{CH3F} = 0.002$. The results taken together

indicate that the predominant photochemical process for the 248 nm photolysis of $CH_3C(O)F$ is the breaking of the C–C bond for which the primary quantum yield of $\varphi_{3a} \approx \Phi_3 = 0.62$ is proposed. The 0.62 QY implies a significant role of photophysical processes in the mechanism, which is surprising at the relatively short wavelength applied and requires further investigations.

To our knowledge, no photochemistry study of acetyl fluoride has been reported, the closest analogy is provided by $CF_3C(O)F$[40][41]. In the more recent work by Bierbrauer et al.[41], the C–C bond cleavage of $CF_3C(O)F$ has been concluded to occur with unity quantum yield at 254 nm. Note that the overall QY of photolysis of acetone is unity at 248 nm (see, e.g. ref. [42] and references therein).

Table 2. Product Quantum Yields for $CH_3C(O)F$ Photolysis at 248 nm ($T = 298 \pm 2$ K); $p(CH_3C(O)F) = 35$ mbar, p(Overall) = 665 mbar, Buffer Gas: N_2.[a]

Scavenger	Φ_{CH4}	Φ_{C2H6}	Φ_{CH3F}	$\Phi_\Sigma = \Phi_{CH4} + 2\Phi_{C2H6} + \Phi_{CH3F}$
–	0.073	0.228	0.050	0.579
222 mbar i-C_5H_{12}	0.184	0.243	0.011	0.682
11 mbar O_2	–	0.017	0.002	–

[a] The presented data are averages of two replicates, thus no errors are given with them.

4. THEORETICAL METHODS

All ab initio calculations were carried out using the Gaussian09 programs.[43] For the sake of computational efficiency, the geometries of all the possible stationary points (e.g., reactants, products, intermediates, and saddle points) were optimized at the economic B3LYP/6-311++G(d,p) level of theory.[44][45] The spin contaminant of the single-reference wavefunction is always less than 0.76 the doublets. The nature of each stationary point was confirmed by the harmonic vibrational frequencies at the same level. Minimum has all real frequencies and transition state has one and only one imaginary frequency. Animation of the imaginary vibrational modes combined with intrinsic reaction coordinate (IRC)[46] calculations confirms the connection of the transition state with its reactants and products.

Subsequently, the geometries and energies of the stationary points for the OH+$CH_3C(O)F$ reaction were re-evaluated using the CBS-QB3[47] and G4[48] methods,
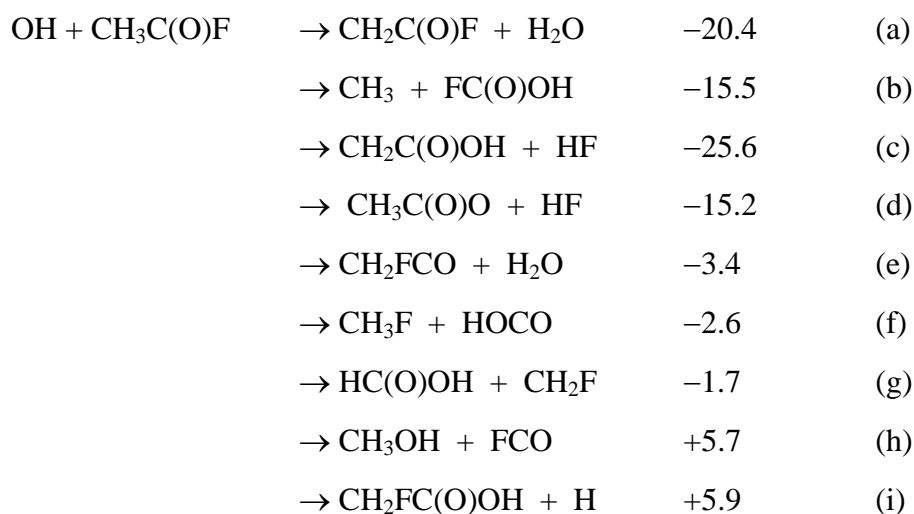
respectively. As default, the CBS-QB3 scheme uses the B3LYP/6-311G(2d,d,p) optimized geometrical parameters and zero-point energies while the G4 method employs the B3LYP/6-31G(2df,p) optimized geometrical parameters and zero-point energies. These two composite approaches have been widely employed in the calculations of the energetic profiles for the radical reactions within the chemical accuracy. [49] [50] [51] Dependence of the geometrical parameters on the levels of theory has been examined using the MP2 [52] or the explicitly correlated restricted open-shell RCCSD(T)-F12 [53] methods for some key stationary points (see Figure SI-6 in SI). Apparently, the deviations from the B3LYP data obtained in the CBS-QB3 and G4 calculations are marginal.

The flexible transition state theory (FTST) as implemented in the Variflex program suite was applied to perform reaction kinetic computations[54]. FTST is a generalized version of variational transition state theory (VTST) and designed specifically to treat large amplitude motion. The minimization of the microscopic rate constants are carried out with respect to the so-called "pivot points" about which the fragments executed their large amplitude motion and thus the most constrictive reaction bottleneck along the optimal reaction coordinates could be obtained. The optimization of these pivot points in FTST can noticeably further lower the rate constant in comparison with those obtained using the conventional VTST.

5. THEORETICAL RESULTS AND DISCUSSION

5.1 Molecular Mechanism of the OH + CH$_3$C(O)F Reaction

A total of eleven energetically accessible product channels have been studied for the reaction of OH with CH$_3$C(O)F, viz.,

$$
\begin{array}{lll}
\mathrm{OH + CH_3C(O)F} & \rightarrow \mathrm{CH_2C(O)F \ + \ H_2O} & -20.4 \quad (a) \\
& \rightarrow \mathrm{CH_3 \ + \ FC(O)OH} & -15.5 \quad (b) \\
& \rightarrow \mathrm{CH_2C(O)OH \ + \ HF} & -25.6 \quad (c) \\
& \rightarrow \mathrm{CH_3C(O)O \ + \ HF} & -15.2 \quad (d) \\
& \rightarrow \mathrm{CH_2FCO \ + \ H_2O} & -3.4 \quad (e) \\
& \rightarrow \mathrm{CH_3F \ + \ HOCO} & -2.6 \quad (f) \\
& \rightarrow \mathrm{HC(O)OH \ + \ CH_2F} & -1.7 \quad (g) \\
& \rightarrow \mathrm{CH_3OH \ + \ FCO} & +5.7 \quad (h) \\
& \rightarrow \mathrm{CH_2FC(O)OH \ + \ H} & +5.9 \quad (i) \\
\end{array}
$$

$$\rightarrow CH_3C(O)OH \ + \ F \qquad +12.9 \qquad\qquad (j)$$

$$\rightarrow CH_2FC(O)H \ + OH \qquad +24.9 \qquad\qquad (k)$$

where channel (a) represents the hydrogen abstraction routes and channels (b)–(k) are involved in the addition mechanism followed by elimination or isomerization paths. All the heats of reaction are reported in the unit of kcal/mol at the CBS-QB3 level of theory. The CBS-QB3 calculated heat of reaction for channel (a) is in good agreement with the experimental value of 20.0 kcal/mol.[55] Moreover, the CBS-QB3 energetics are in fairly good agreement with the G4 data since the absolute average deviation is less than 1 kcal/mol. The CBS-QB3 geometries and energies are used in the following discussions unless stated otherwise.

5.1.1 Hydrogen Abstraction Mechanism

The hydrogen abstraction occurs between the OH radical and one of the hydrogen atoms of the methyl group of $CH_3C(O)F$. The reaction proceeds via intermolecular hydrogen-bond complexes. All the prereactive and postreactive complexes have been explored for completeness along the reaction paths, as shown in Figures 6 and 7.

Two prereactive complexes, namely, RC1 and RC2, exist at the entrance channel. RC1 involves a nearly planar cyclic structure with two hydrogen bonds, where the OH radical acts as both proton donor to the carbonyl O atom and proton acceptor from the methyl group. The binding energy of RC1 was calculated to be 3.5 kcal/mol, which is very close to that of water dimer.[56] TS1a is the transition state following RC1. One of the CH bonds is stretched collinearly toward the OH radical to form the H_2O molecule. The breaking CH bond and the forming OH bond are very similar in the distances. The OH...O hydrogen bond tends to be broken as indicated by the elongated intermolecular distance. However, the hydrogen bonds are fully recovered after abstraction in the postreactive complex PC1 formed between H_2O and $CH_2C(O)F$. The barrier height for TS1a is 7.5 kcal/mol (4.0 with respect to reactants).
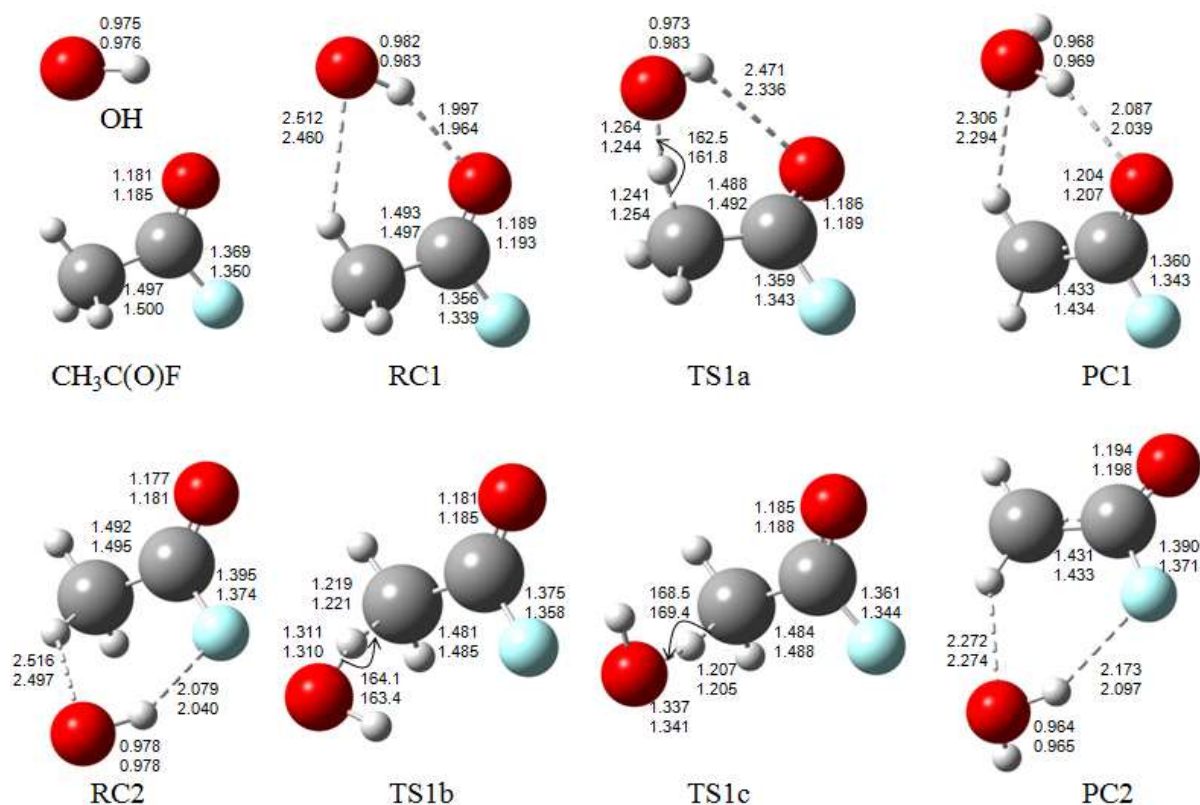
Figure 6. Geometries of the species involved in the hydrogen abstraction mechanism of the OH + CH$_3$C(O)F reaction optimized at the CBS-QB3 (upper numbers) and G4 (lower numbers) levels of theory. Distances are in Å and angles are in degrees.

RC2 is a much weaker prereactive complex than RC1. The binding energy of RC2 is only half of that of RC1. As shown in Figure 7, RC2 involves a flexible cyclic geometry with two weak out-of-the-plane intermolecular hydrogen bonds, as indicated by the interacting distances. Interestingly, such a weak interacting mode remains in the postreactive complex PC2, the energy of which is about 1.4 kcal/mol higher than that of PC1. Two transition states have been found starting from RC2, as distinguished by the orientations of the OH radical. Both TS1b and TS1c have been characterized to be true saddle points for the H-abstraction reaction. The corresponding imaginary vibrational frequencies are 1048 and 845 cm^{-1} for TS1b and TS1c, respectively. The internal rotation of the OH moiety is characterized by the positive normal vibrational frequencies of 231 and 128 cm^{-1}, respectively. The IRC calculations further unambiguously confirm the distinct minimum energy reaction paths for TS1b and TS1c. Moreover, the geometries of TS1b and TS1c do show some difference. The breaking CH bond in TS1b is about 0.02 Å longer than that in TS1c, whereas the length of the forming HO bond is in reverse. In comparison with the in-the-plane TS1a structure, both

TS1b and TS1c are more reactant-like, as indicated by the longer OH bonds and the shorter CH bonds. Accordingly, the barrier heights for TS1b and TS1c are 5.4 and 5.9 kcal/mol, respectively, which are about 2 kcal/mol lower than the barrier at TS1a. However, the relative energies of TS1a, TS1b, and TS1c with respect to the reactants are very close to each other. It is noteworthy that the net barrier height for the lowest TS1b structure is only 3.7 kcal/mol. Therefore, the three H-abstraction routes could be effectively competitive.
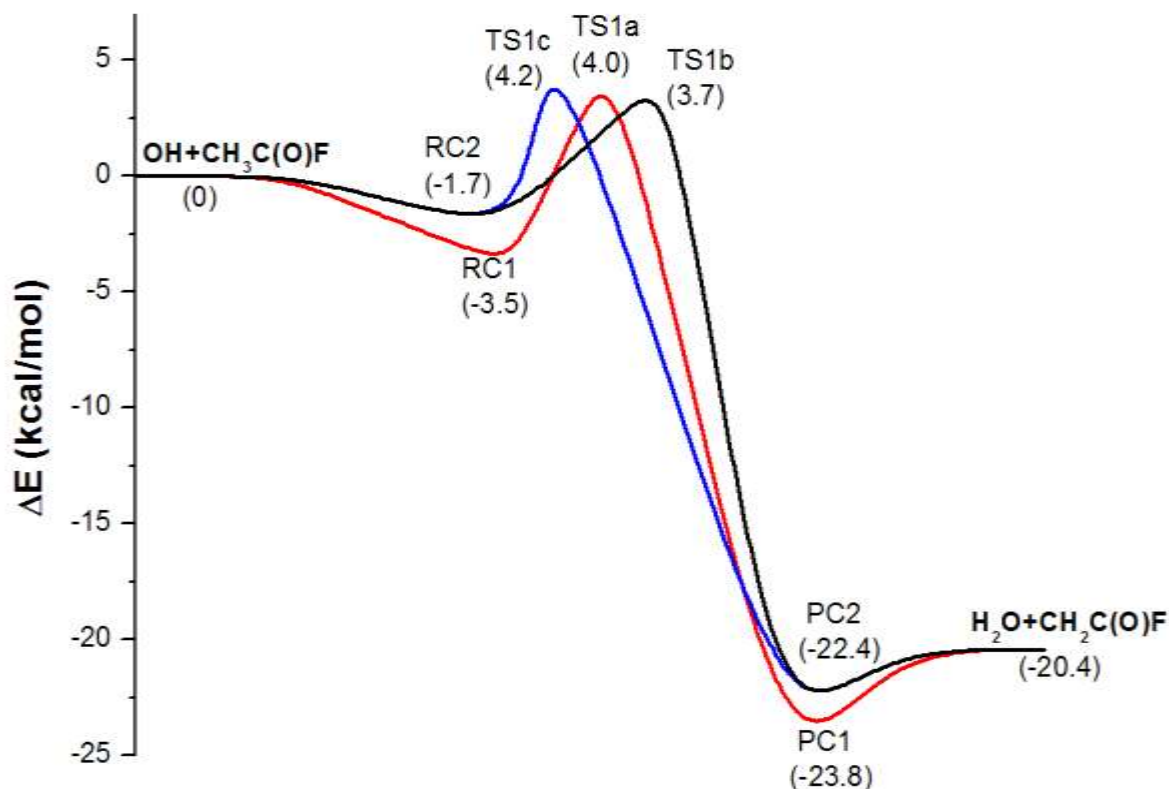
Figure 7. The energetic profile for the hydrogen abstraction mechanism of the OH + CH$_3$C(O)F reaction calculated at the CBS-QB3 level.

In order to clarify the F-substituent effect on the OH reactivity, the reaction of OH with acetone has also been calculated at the CBS-QB3 level of theory in our present work (see Figure SI-8 in SI). The calculated net barrier heights of the hydrogen abstraction pathways for OH + CH$_3$C(O)CH$_3$ are generally lower by ~3 kcal/mol than those computed for the OH + CH$_3$C(O)F reaction. Consequently, the F-substituent is predicted to reduce the reactivity significantly, as demonstrated by the much smaller rate coefficients for the OH + CH$_3$C(O)F reaction. More interestingly, the in-the-plane H-abstraction route in the OH + CH$_3$C(O)CH$_3$ reaction involves the lowest barrier, but the out-of-plane abstraction possesses the highest barrier, which is contrary to the barrier orders for the OH + CH$_3$C(O)F reaction.

On the other hand, TS1a-c for the H-abstraction routes might be viewed geometrically as only one saddle point involving either the OH internal rotation or the CH$_3$OH torsion. Further calculations to map the multidimensional potential energy surfaces for the H-abstraction mechanim is desired to clarify whether these are the different transition states or just different parts of the same transition state dividing surface.

5.1.2 Addition/Elimination Mechanism

Besides the H-abstraction pathways, the reaction OH + CH$_3$C(O)F could take place via attack of OH on the carbonyl group of the acetyl fluoride molecule, forming the intermediate IM1, as shown in Figures 8 and 9.

The addition reaction of OH to the >C=O group proceeds via an intermolecular hydrogen-bond complex, denoted as RC3 in Figure 8. The hydrogen bonding occurs between the carbonyl O atom and the hydrogen atom of OH. Although only one H-bond exists in RC3, its binding energy is nearly equal to that of RC1. TS2 is the transition state for the addition path. Apparently, TS2 is an early barrier. The forming C...O bond is about 0.5 Å longer than the equilibrium C-O bond in IM1. Meanwhile, the breaking C=O bond is only slightly elongated and the bond remains largely of double bond nature. The barrier height for TS2 is 10.2 kcal/mol, leading to the net barrier of up to 6.8 kcal/mol, which is more than 3 kcal/mol higher than that for the hydrogen abstraction paths. The intermediate IM1 represents a substituted methoxy radical structure and is only 4.5 kcal/mol more stable than the prereactive H-bond complex RC3. The weakest bond in IM1 is C-C, which breaks apart to form the CH$_3$ radical and FC(O)OH via TS3. The energy of TS3 is 6.6 kcal/mol lower than that of TS2. Apparently, the OH-addition is the rate-determining step for the addition/elimination mechanisms.

In comparison with the OH + CH$_3$C(O)CH$_3$ reaction, (see e.g, refs. [17 20 22 23]) the OH + CH$_3$C(O)F reaction possesses about two times higher barrier for the OH-addition route, resulting from the strong electron withdrawing character of the F-substituent. Moreover, the intermediate IM1 becomes less stable for the acetyl fluoride reaction. Nevertheless, the C-C bond energy appears to be unaffected since the barriers for the C–C bond cleavage remain ~7 kcal/mol.

As illustrated in Figure 9 (see Figure SI-9 in SI for geometries), the other bond fission or isomerization routes starting from IM1 are less feasible because either the involved

barriers along the minimum energy paths are too high (e.g., > 10 kcal/mol) to be important or the respective production channels are endothermic. Therefore, the dominant products of the addition/elimination mechanism should be only $CH_3 + FC(O)OH$. To this end it is noted that there exists a S_N2-type displacement pathway for the $OH + CH_3C(O)F$ reaction as well, leading to $CH_3 + FC(O)OH$ directly. However, the barrier for such a pathway is as high as 41 kcal/mol and thus it is negligible.

It is worth noting that beside the H-abstraction pathways that occur through prereactive complexes as discussed in Section 5.1.1, the $CH_2C(O)F + H_2O$ products could be formed via the four-member-ring barrier from IM1. The calculated barrier is more than 50 kcal/mol. Therefore, such an indirect type of H-abstraction involving the IM1 adduct could be ruled out safely.
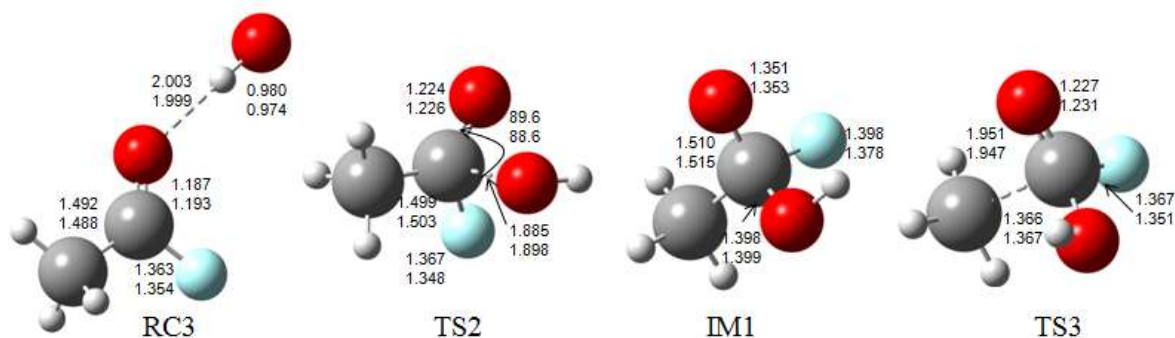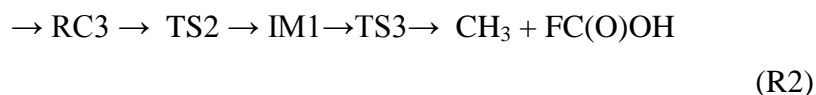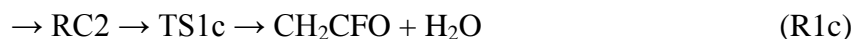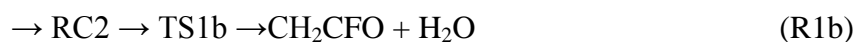

Figure 8. Geometries of the key species involved in the addition/elimination mechanism for the $OH + CH_3C(O)F$ reaction optimized at the CBS-QB3 (upper numbers) and G4 (lower numbers) levels of theory. Distances are in Å and angles are in degrees.
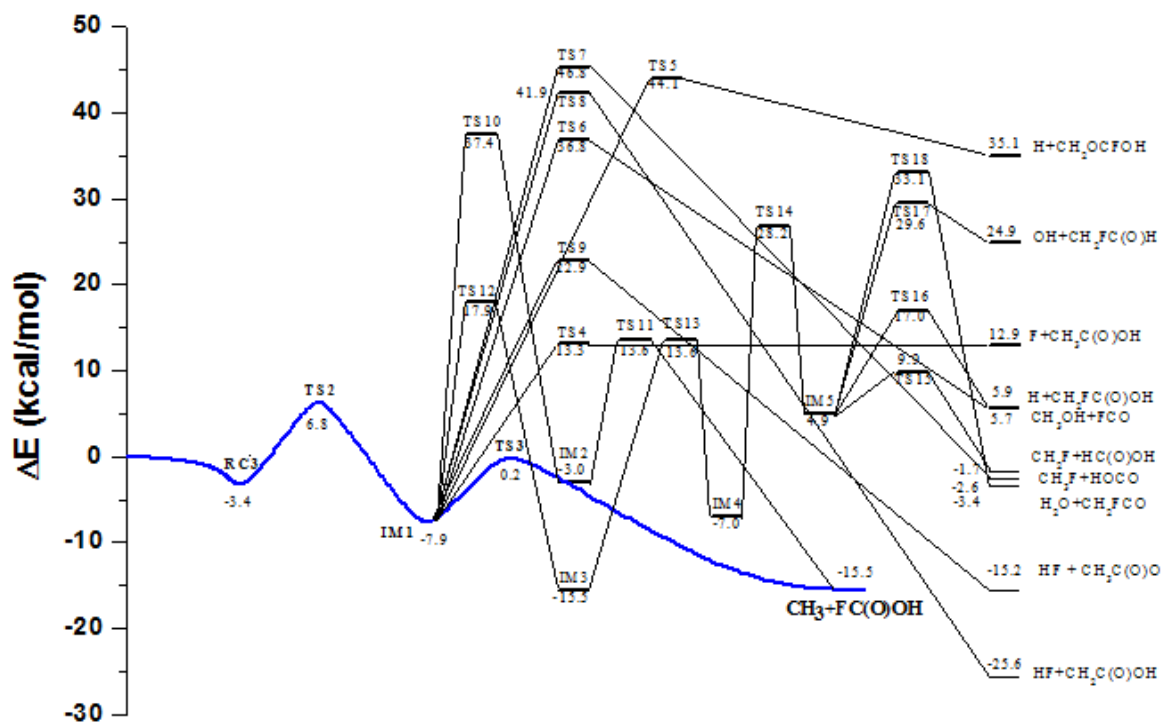
Figure 9. The energetic profile for the addition/elimination mechanism of the OH + CH$_3$C(O)F reaction calculated at the CBS-QB3 level.

5.2 Theoretical Rate Coefficients

As demonstrated in Figures 7 and 9, the predominant energetic routes for the OH + CH$_3$C(O)F reaction can be summarized as follows:

$$OH + CH_3C(O)F \rightarrow RC1 \rightarrow TS1a \rightarrow CH_2CFO + H_2O \qquad (R1a)$$

$$\rightarrow RC2 \rightarrow TS1b \rightarrow CH_2CFO + H_2O \qquad (R1b)$$

$$\rightarrow RC2 \rightarrow TS1c \rightarrow CH_2CFO + H_2O \qquad (R1c)$$

$$\rightarrow RC3 \rightarrow TS2 \rightarrow IM1 \rightarrow TS3 \rightarrow CH_3 + FC(O)OH$$

$$(R2)$$

On the basis of the ab initio CBS-QB3 and G4 geometries and energies for the species involved in both H-abstraction and addition/elimination mechanisms, the temperature-dependent rate coefficients for the title reaction were calculated using the flexible transition state theory as realized in the Variflex program[54]. The prereactive H-bonded complexes have been considered explicitly in the rate calculations. The energetic profiles for the formation of RC1, RC2, and RC3 were obtained by the partial optimization technique. The respective

26

collective reaction coordinates (e.g., the approaching HO...HCH$_2$ moieties) for the interaction potentials of the two reactant fragments were scanned successively with the centre-of-mass separation distance ranging from 2.5 to 8.0 Å with a step size of 0.1 Å at the CBS-QB3 level. The ab initio energies were used straightforwardly in the variational treatments of the dynamic bottlenecks for the association by interpolation. Although the full-dimensional potential surface is desired, the current relaxed minimum energy paths should be good enough to account for the contributions of the association dynamical bottleneck on the overall rate coefficients. It has been shown that under the low-pressure conditions the influence of the barrierless association region is only marginal as long as the adiabatic potential energy barrier of the hydrogen abstraction saddle point is positive with respect to the reactants,[57] as it is exactly the case in the present work.

Only the association paths of OH with CH$_3$C(O)F to form RCs have been treated implicitly using the flexible variational transition state theory. The other reaction routes are considered using the conventional transition state theory without variation. The rigid rotor harmonic oscillator (RRHO) approximation was employed to evaluate sum and densities of states for the transition states TS1a, TS1b, TS1c, TS2, and TS3 in view of the tight characters of these TSs. Quantum tunnelling was estimated using the one-dimensional Eckart potentials [58]. Special attention has been paid to the hindered internal rotors for transition states and complexes. The essential internal rotors are identified in normal mode vibrational analysis as implemented in the Gaussian09 program [43] [59]. The normal vibrational modes corresponding to internal rotations are identified by solving the vibrational problem for the constrained system in the redundant internal coordinates. The atomic composition of the rotating groups is determined automatically without any user's intervention or expertise. The kinetic energy matrix for internal rotation is given by the constrained Wilson-G matrix. Such an approximation has been demonstrated to perform well in the calculation of partition functions for a wide range of temperatures. The sum of states of the one-dimensional hindered rotors were calculated using the simple cosine function, i.e., $V = V_0 \times \cos(m \times \phi)$, where V_0 is the barrier height for the internal rotor and m is the multiplicity of the rotations.

The rate coefficients were obtained using the one-dimensional master equation method at the energy and angular momentum (E/J) resolved level. The bath gas is helium (p = 2.5 mbar) and a simple exponential down energy transfer model was used for the collisional deactivation. The energy transfer parameter was set arbitrarily to be $\alpha = 100$ cm^{-1}.

It has been confirmed that the rate coefficient is insensitive to this empirical parameter by preliminary trial calculations.

The calculated rate coefficients in the temperature range 200-1000 K have been presented in Figure 10 in comparison with the experimental data. Firstly, the theoretical rate coefficients are in very good agreement with the experimental data in the temperature range 300–410 K: the average deviation between experiment and theory is –34% and 32% for the (CBS-QB3)–FTST and G4-FTST computations, respectively. Considering the possible uncertainties in the CBS-QB3 and G4 energetic data, the overlap between the measured data and the ab initio predicted data demonstrates the reliability of the present mechanistic and kinetic calculations. Secondly, it is evident that the contribution of the addition/elimination routes is smaller than that of the hydrogen abstraction by at least two orders of magnitude. Therefore, the association of OH with $CH_3C(O)F$ might play a negligible role within the temperature range of our concern. Thirdly, the overall rate coefficients show the typical non-Arrhenius behavior. At temperatures below 500 K, the in-the-plane H-abstraction (TS1a) route dominates the reaction. It was ascribed to the significant tunnelling effect of TS1a at the low temperature range. Although the transition state TS1a is the highest barrier among the three H-abstraction bottlenecks, its profile of the minimum energy path is the thinnest one (see Figure SI-10 in SI) together with the largest imaginary vibrational frequency 1312i cm^{-1}. The profiles of the minimum energy path for the other two out-of-the-plane barriers, TS1b and TS1c, are much wider and the imaginary frequencies are 1048i and 845i cm^{-1}, respectively. As the temperature increases, the tunnelling effect decreases rapidly and thus the out-of-the-plane H-abstraction starts to be competitive in view of their slightly lower barrier heights (~3.7–4.0 kcal/mol).
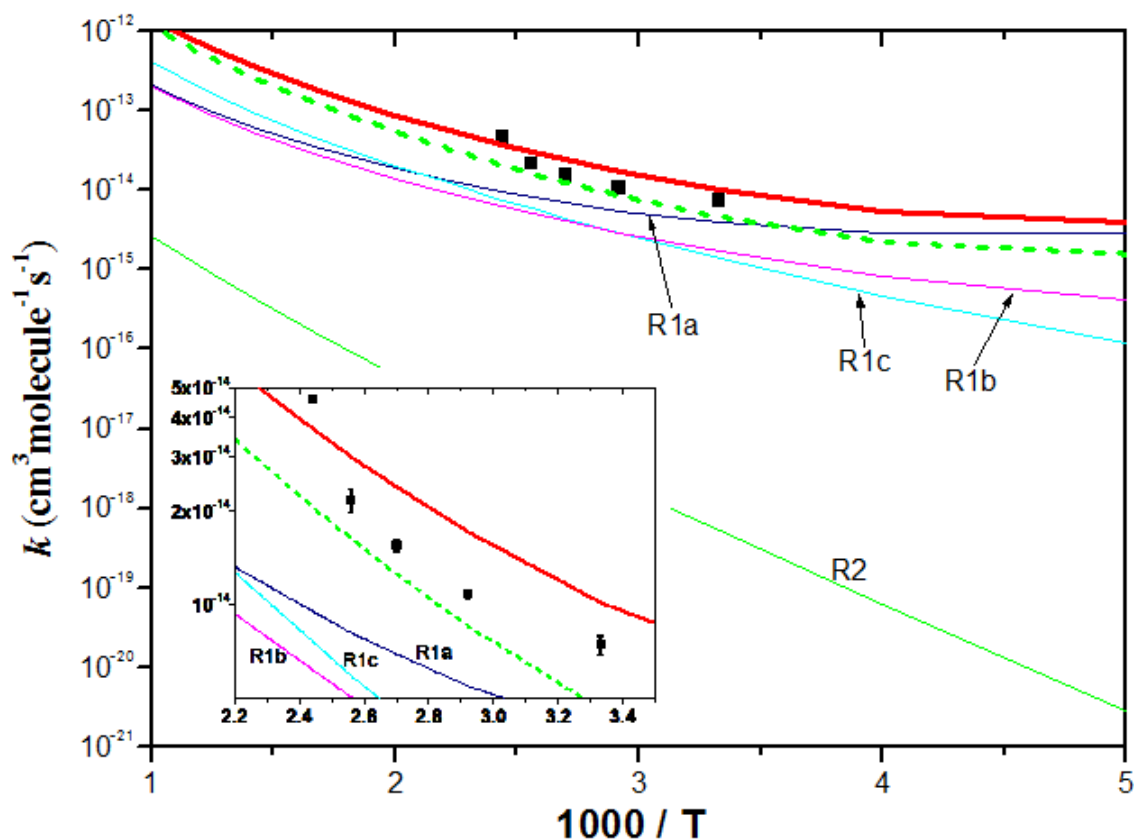
Figure 10. The calculated overall (thick lines) and channel-specific (thin lines) rate coefficients for the OH + CH$_3$C(O)F reaction. Squares: experimental data. Solid line: at the CBS-QB3 level. Dashed line: at the G4 level. The channel-specific rate coefficients are calculated at the CBS-QB3 level. The comparison between theory and experiment are highlighted in the inserts for clearness.

6. IMPLICATIONS FOR TROPOSPHERIC CHEMISTRY

The k_2 value determined at laboratory temperature in our experiments can be used to estimate the tropospheric lifetime of acetyl fluoride with respect to its reaction with OH radical, τ_{OH}. With an average global hydroxyl radical concentration of [OH]$_{global}$ = 1 × 10^6 radicals cm^{-3} (24 h average),[60] the tropospheric lifetime of τ_{OH} (AcF) ≈ 1 / (k_2(300 K) × [OH]$_{global}$) = 4.3 years is estimated. The same simple estimation gives 61 days for the lifetime of the parent molecule C$_2$H$_5$F (HFC-161) by using our measured k_1(298 K). (More sophisticated calculations give τ_{OH} (C$_2$H5F) = 66 days.[5])

Rattigan et al. have applied a two-dimensional (latitude, height) photochemical model to calculate the globally averaged photochemical lifetime of τ_{phot} = 41 years for acetyl

fluoride in the troposphere.[39] The authors used the absorption spectrum they determined (see also in Section 3.4) and assumed a photolysis QY of unity over the whole absorption range. In view of our own results, τ_{phot} can even be longer in particular that we could not detect light absorption for AcF in the actinic region ($\lambda > 290$ nm).

Both homogeneous processes studied, i.e., the reaction with OH and photolysis, are very slow for $CH_3C(O)F$. Therefore, and on analogy with carbonyl halides and other haloacetyl halides[61][62], the tropospheric removal of acetyl fluoride is anticipated to occur mostly by uptake in the aqueous phase; an upper limit of 30-day lifetime[62] has been proposed for CCl_2O, CF_2O, $CCl_3C(O)Cl$, $CF_3C(O)F$ and $CF_3C(O)Cl$. Similarly to these halides, the rate of removal of $CH_3C(O)F$ depends on the Henry's law solubility coefficient, H_{AcF}, and the hydrolysis rate coefficient, k_{hydrol}. Unfortunately, neither of these parameters is known accurately: k_{hydrol} values that have been reported differ by more than two orders of magnitude[63][64] and there is no H_{AcF} available. Here we accept the results of the more recent and more detailed study by Bunton and Fendler[64] and take $k_{hydrol.}= 5.8 \times 10^{-3}$ s^{-1} ($T = 278$ K, pH = 7). Moreover, the Henry's law coefficient of acetyl fluoride is assumed to be equal with that of $CF_3C(O)F$, $H_{AcF} = H_{CH3C(O)F} = 3$ M atm^{-1} [65][66]. By making use of these parameters and utilizing the correlation diagram reported by De Bryn et al. [62] (Figure 6 in ref [62]) we estimate $\tau_{aq} \approx 100$ days for the heterogenous removal of acetyl fluoride in the troposphere (cloud processing + ocean uptake). While this estimation is quite uncertain, it allows the conclusion to be made that aquatic processes are by far the most important in depleting acetyl fluoride in the troposphere. Also, that the atmospheric lifetime of AcF is likely of comparable magnitude to that of its parent molecule C_2H_5F (HFC-161) and so no substantial build-up of this oxidation intermediate is probable. Clearly, however, measurements of the $CH_3C(O)F$ hydrolysis rate and Henry's law coefficients are required in order to propose more accurate τ_{aq}. Acetyl fluoride hydrolyses in cloud droplets, $CH_3C(O)F + H_2O \rightarrow CH_3C(O)OH + HF$ [64], and washes out from the gas phase causing negligible impact on the environment. In conclusion, from an environmental point of view it appears that C_2H_5F(HFC-161) would be an acceptable substitute for the high GWP refrigerants.

7. SUMMARY AND CONCLUSIONS

We report experimental and theoretical results for the kinetics and mechanism of the reaction of OH with acetyl fluoride the first time. Fluorine substitution, due to the strong negative inductive effect, is found to reduce the reactivity with OH very significantly. As for instance, the rate coefficient for the OH + $CH_3C(O)CH_3$ reaction is larger by two orders of magnitude than that of the OH + $CH_3C(O)F$ reaction at room temperature.

Ab initio CBS-QB3 and G4 calculations reveal two types of mechanisms for the title reaction, namely, hydrogen abstraction and addition/elimination. Both reaction pathways involve prereactive H-bond complexes. The experimental rate coefficients have been well reproduced by the variational transition state theory on the basis of the ab initio structures and energetics. It is found that the hydrogen abstraction always dominates the OH + $CH_3C(O)F$ reaction in the temperature range 200–1000 K. The tunneling effect due to the in-the-plane H-abstraction dynamic bottleneck accounts for the non-Arrhenius behavior of the rate coefficients at temperatures below 500 K. The major nascent products are predicted to be H_2O and the $CH_2C(O)F$ radical.

Substitution of the CH_3 group in $CH_3C(O)CH_3$ for F-atom shifts the absorption spectrum to shorter wavelengths very substantially, but the predominant primary photochemical process for $CH_3C(O)F$ at 248 nm remains the C–C bond cleavage similarly to acetone.

Acetyl fluoride is a reaction intermediate in the degradation of C_2H_5F (HFC-161) in the atmosphere. Its tropospheric removal is concluded to occur via uptake in cloud droplets and hydrolysis to acetic acid, likely causing negligible environmental impact.

ASSOCIATED CONTENT

Supporting Information

Additional pseudo-first order plots for OH + $CH_3C(O)F$ Beer-Lambert plots for $CH_3C(O)F$, Table of absorption cross sections of $CH_3C(O)F$ vs. wavelength, Optimized geometries, CBS-QB3 and G4 energies, Profiles of the minimum energy paths. This material is available free of charge via the Internet at http://pubs.acs.org.

AUTHOR INFORMATION

Corresponding Authors

*E-mail: baoshan@whu.edu.cn.

*E-mail: dobe.sandor@ttk.mta.hu.

Notes

The authors declare no competing financial interest.

REFERENCES

1.   Velders, G.; Andersen, S.; Daniel, J.; Fahey, D.; McFarland, M., The Importance of the Montreal Protocol in Protecting Climate. *Proc. Natl. Acad. Sci. U. S. A.* **2007,** *104* (12), 4814-4819.

2.   Velders, G.; Ravishankara, A.; Miller, M.; Molina, M.; Alcamo, J.; Daniel, J.; Fahey, D.; Montzka, S.; Reimann, S., Preserving Montreal Protocol Climate Benefits by Limiting HFCs. *Science* **2012,** *335*, 922-923.

3.   Mota-Babiloni, A.; Navarro-Esbrí, J.; Barragán-Cervera, Á.; Molés, F.; Peris, B., Analysis Based on EU Regulation No 517 / 2014 of New HFC / HFO Mixtures as Alternatives of High GWP Refrigerants in Refrigeration and HVAC Systems. *Int. J. Refrigeration,* **2015,** *52*, 21-31.

4.   Thompson, M., Climate Change Regulation and the Next Generation of Refrigerants. http://www.trane.com/commercial/uploads/pdf/cso/138/Refrigerants.pdf. 2014.

5.   Hodnebrog, O.; Etminan, M.; Fuglestvedt, J. S.; Marston, G.; Myhre, G.; Nielsen, C. J.; Shine, K. P.; Wallington, T. J., Global Warming Potentials and Radiative Efficiencies of Halocarbons and Related Compounds: A Comprehensive Review. *Rev. Geophys.* **2013,** *51*, 300-378.

6.   Xuan, Y.; Chen, G., Experimental Study on HFC-161 Mixture as an Alternative Refrigerant to R502. *Int. J. Refrigeration* **2005,** *28*, 436-441.

7.   Han, X. H.; Qiu, Y.; Li, P.; Xu, Y. J.; Wang, Q.; Chen, G. M., Cycle Performance Studies on HFC-161 in a Small-scale Refrigeration System as an Alternative Refrigerant to HFC-410A. *Energy and Buildings* **2012,** *44*, 33-38.

8.   Han, X. H.; Li, P.; Xu, Y. J.; Zhang, Y. J.; Wang, Q.; Chen, G. M., Cycle Performance of the Mixture HFC-161 + HFC-134a as the Substitution of HFC-134a. *Int. J. Refrigeration* **2013,** *36*, 913-920.

9.   Sun, H.; He, H.; Gong, H.; Pan, X.; Li, Z.; Wang, R., Theoretical Investigation into the Hydrogen Abstraction Reaction of CH_3CH_2F (HFC-161) with OH. *Chem. Phys.* **2006,** *327* (1), 91-97.

10.   Singleton, D. L.; Paraskevopoulos, G.; Irwin, R. S., Reaction of OH with CH_3CH_2F - The Extent of H Abstraction from the Alpha and Beta Positions. *J. Phys. Chem.* **1980,** *84*, 2339-2343.

11.   Taketani, F.; T., N.; Takahashi, K.; Y., M.; Hurley, M. D.; Wallington, T. J.; Toft, A.; Andersen, M. P. S., Atmospheric Chemistry of CH_3CHF_2 (HFC-152a): Kinetics, Mechanisms, and Products of Cl Atom- and OH Radical-Initiated Oxidation in the Presence and Absence of NO*x*. *J. Phys. Chem. A* **2005***, 109,* 9061-9069.

12.   HFCs: A Critical Link in Protecting Climate and the Ozone Layer. United Nations Environment Programme (UNEP). 2011; p 36.

13.   Wollenhaupt, M.; Carl, S. A.; Horowitz, A.; Crowley, J. N., Rate Coefficients for Reaction of OH with Acetone between 202 and 395 K. *J. Phys. Chem. A* **2000,** *104*, 2695-2705.

14.   Vasvári, G.; Szilágyi, I.; Bencsura, Á.; Dóbé, S.; Bérces, T.; Henon, E.; Canneaux, S.; Bohr, F., Reaction and Complex Formation between OH Radical and Acetone. *Phys. Chem. Chem.l Phys.* **2001,** *3*, 551-555.

15.   Gierczak, T.; Gilles, M.; Bauerle, S.; Ravishankara, A., Reaction of Hydroxyl radical with Acetone. 1. Kinetics of the Reactions of OH, OD, and (OH)-O-18 with Acetone and Acetone-d(6). *J. Phys. Chem. A* **2003,** *107*, 5014-5020.

16.   Talukdar, R.; Gierczak, T.; McCabe, D.; Ravishankara, A., Reaction of Hydroxyl Radical with Acetone. 2. Products and Reaction Mechanism. *J. Phys. Chem. A* **2003,** *107*, 5021-5032.

17.   Vandenberk, S.; Vereecken, L.; Peeters, J., The Acetic Acid Forming Channel in the Acetone Plus OH Reaction: A Combined Experimental and Theoretical Investigation. *Phys. Chem. Chem. Phys.* **2002,** *4*, 461-466.

18.   Raff, J.; Stevens, P.; Hites, R., Relative Rate and Product Studies of the OH - Acetone Reaction. *J. Phys. Chem. A* **2005,** *109*, 4728-4735.

19.   Davis, M.; Drake, W.; Vimal, D.; Stevens, P., Experimental and Theoretical Studies of the Kinetics of the Reactions of OH and OD with Acetone and Acetone-d(6) at Low Pressure. *J. Photochem. Photobiol. A-Chemistry* **2005,** *176*, 162-171.

20.   Yamada, T.; Taylor, P.; Goumri, A.; Marshall, P., The Reaction of OH with Acetone and Acetone-d(6) from 298 to 832 K: Rate Coefficients and Mechanism. *J. Chem. Phys.* **2003,** *119*, 10600-10606.

21.   Turpin, E.; Fittschen, C.; Tomas, A.; Devolder, P., Reaction of OH Radicals with Acetone: Determination of the Branching Ratio for the abstraction pathway at 298 K and 1 Torr. *J. Atm. Chem.* **2003,** *46*, 1-13.

22.   Masgrau, L.; Gonzalez-Lafont, A.; Lluch, J., Variational Transition-state Theory rate Constant Calculations with Multidimensional Tunneling Corrections of the Reaction of Acetone with OH. *J. Phys. Chem. A* **2002,** *106*, 11760-11770.

23.   Henon, E.; Canneaux, S.; Bohr, F.; Dóbé, S., Features of the Potential Energy Surface for the Reaction of OH Radical with Acetone. *Phys. Chem. Chem. Phys.* **2003,** *5*, 333-341.

24.   Caralp, F.; Forst, W.; Henon, E.; Bergeat, A.; Bohr, F., Tunneling in the Reaction of Acetone with OH. *Phys. Chem. Chem. Phys.* **2006,** *8*, 1072-1078.

25.   Iuga, C.; Alvarez-Idaboy, J.; Vivier-Bunge, A., On the Possible Catalytic Role of a Single Water molecule in the Acetone Plus OH Gas Phase Reaction: a Theoretical Pseudo-second-order Kinetics Study. *Theor. Chem. Acc.* **2011,** *129*, 209-217.

26.   Sander, S. P.; Friedl, R. R.; Barker, J. R.; Golden, D. M.; Kurylo, M. J.; Wine, P. H.; Abbatt, J. P. D.; Burkholder, J. B.; Kolb, C. E.; Moortgat, et al., Chemical Kinetics and Photochemical Data for Use in Atmospheric Studies. *JPL Publication 10-6* **2011,** *Evaluation Number 17* (Jet Propulsion Laboratory, Pasadena, http://jpldataeval.jpl.nasa.gov).

27.   Imrik, K.; Farkas, E.; Vasvári, G.; Szilágyi, I.; Sarzynski, D.; Dóbé, S.; Bérces, T.; Márta, F., Laser Spectrometry and Kinetics of Selected Elementary Reactions of the Acetonyl Radical. *Phys. Chem. Chem. Phys.***2004,** *6*, 3958-3968.

28.   Zügner, G. L. Atmospheric Chemistry and Climate Coupling: Reaction Kinetics and Photochemical Study of Selected Fluorinated and Oxygen Containing Organic Molecules. PhD thesis, Budapest University of Technology and Economics, Budapest, 2014.

29.   Nádasdi, R.; Zügner, G. L.; Farkas, M.; Dóbé, S.; Maeda, S.; Morokuma, K., Photochemistry of Methyl Ethyl Ketone: Quantum Yields and S(1)/S(0)-Diradical Mechanism of Photodissociation. *Chemphyschem* **2010,** *11*, 3883-3895.

30.   Gierczak, T.; Burkholder, J. B.; Bauerle, S.; Ravishankara, A. R., Photochemistry of Acetone under Tropospheric Conditions. *Chem. Phys.* **1998,** *231*, 229-244.

31.   Hoyermann, K. H., Physical Chemistry - An Advanced Treatise. Vol. VI B/Kinetics of Gas Reactions. Academic Press: New York, 1975; Vol. VI B.

32.   Baasandorj, M.; Griffith, S.; Dusanter, S.; Stevens, P., Experimental and Theoretical Studies of the Kinetics of the OH plus Hydroxyacetone Reaction As a Function of Temperature. *J. Phys. Chem. A* **2009**, 10495-10502.

33.   Szabó, E.; Djehiche, M.; Riva, M.; Fittschen, C.; Coddeville, P.; Sarzyński, D.; Tomas, A.; Dóbé, S., Atmospheric Chemistry of 2,3-Pentanedione: Photolysis and Reaction with OH Radicals. *J. Phys. Chem. A* **2011,** *115*, 9160-9168.

34.   Kwok, E.; Atkinson, R., Estimation of Hydroxyl Radical Reaction Rate Constants for Gas Phase Organic Compounds Using a Structure-reactivity Relationship − an Update. *Atmos. Environ.* **1995**, *29*, 1685-1695.

35.   Kurylo, M. J.; Orkin, V. L., Determination of Atmospheric Lifetimes via Measurement of OH Radical Kinetics. *Chem. Rev.* 2003, *103*, 5049–5076.

36.   Kozlov, S.; Orkin, V.; Kurylo, M., An Investigation of the Reactivity of OH with Fluoroethanes: CH_3CH_2F (HFC-161), CH_2FCH_2F (HFC-152), and CH_3CHF_2 (HFC-152a). *J. Phys. Chem. A* **2003,** *107*, 2239-2246.

37.   Orkin, V.; Khamaganov, V.; Martynova, L.; Kurylo, M., High-Accuracy Measurements of ·OH Rate Constants and IR and UV Absorption Spectra: Ethanol and Partially Fluorinated Ethyl Alcohols. *J. Phys. Chem. A* **2011,** *115*, 8656-8668.

38.   Khamaganov, V.; Bui, V.; Carl, S.; Peeters, J., Absolute Rate Coefficient of the OH + $CH_3C(O)OH$ Reaction at T = 287-802 K. The Two Faces of Pre-reactive H-bonding. *J. Phys. Chem. A* **2006,** *110*, 12852-12859.

39.	Rattigan, O.; Wild, O.; Jones, R.; Cox, R., Temperature-dependent Absorption Cross-Sections of CF_3COCl, CF_3COF, CH_3COF, CCl_3CHO and CF_3COOH. *J. Photochem. Photobiol. A-Chemistry* **1993**, *73*, 1-9.

40.	Weibel, D.; Devohringer, C.; Staricco, E.; Destaricco, E., Quantum Yield of Photolysis of Perfluoroacetyl Fluoride Vapor – Possible Source of CF_3 Radicals. *J. Photochem. Photobiol. A-Chemistry* **1992,** *63*, 1-6.

41.	Bierbrauer, K.; Chiappero, M.; Malanca, F.; Arguello, G., Photochemistry of Perfluoroacetyl Fluoride - Kinetics of the Reaction between CF_3 and FCO radicals. *J. Photochem. Photobiol. A - Chemistry* **1999,** *122*, 73-78.

42.	Khamaganov, V. G.; Karunanandan, R.; Horowitz, A.; Dillon, T. J.; Crowley, J. N., Photolysis of $CH_3C(O)CH_3$ at 248 and 266 nm: Pressure and Temperature Dependent Overall Quantum Yields. *Phys. Chem. Chem. Phys.* **2009,** *11*, 6173-6181.

43.	Frisch, M. J. et al. *Gaussian 09,*, Gaussian, Inc.: Wallingford CT, 2009.

44.	Becke, A., Density-functional Thermochemistry. 3. The Role of Exact Exchange. *J. Chem. Phys.* **1993,** *98*, 5648-5652.

45.	Lee, C.; Yang, W.; Parr, R., Development of the Colle-Salvetti correlation-energy formula into a functional of the electron-density. *Phys. Rev. B* **1988,** *37* (2), 785-789.

46.	Gonzalez, C.; Schlegel, H., An Improved Algorithm for Reaction-path Following. *J. Chem.Phys.* **1989,** *90*, 2154-2161.

47.	Montgomery, J.; Frisch, M.; Ochterski, J.; Petersson, G., A Complete Basis Set Model Chemistry. VI. Use of Density Functional Geometries and Frequencies. *J. Chem. Phys.* **1999,** *110*, 2822-2827.

48.	Curtiss, L.; Redfern, P.; Raghavachari, K., Gaussian-4 Theory. *J. Chem. Phys.* **2007,** *126*, 084108.

49.	Kuwata, K.; Hasson, A.; Dickinson, R.; Petersen, E.; Valin, L., Quantum Chemical and Master Equation Simulations of the Oxidation and Isomerization of Vinoxy Radicals. *J. Pys. Chem. A* **2005,** *109*, 2514-2524.

50.	Chakravarty, H.; Fernandes, R., Reaction Kinetics of Hydrogen Abstraction Reactions by Hydroperoxyl Radical from 2-Methyltetrahydrofuran and 2,5-Dimethyltetrahydrofuran. *J. Phys. Chem. A* **2013,** *117*, 5028-5041.

51.	Lin, C.; Hodgson, J.; Namazian, M.; Coote, M., Comparison of G3 and G4 Theories for Radical Addition and Abstraction Reactions. *J. Phys. Chem. A* **2009,** *113*, 3690-3697.

52.	Møller, Ch.; Plesset, M. S., Note on an Approximation Treatment for Many-Electron Systems. *Phys. Rev.* **1934,** *46*, 618-622.

53.	Knizia, G.; Adler, T.; Werner, H., Simplified CCSD(T)-F12 Methods: Theory and Benchmarks. *J. Chem. Phys.* **2009,** *130*, 054104.

54.   Klippenstein, S. J.; Wagner, A. F.; Dunbar, R. C.; Wardlaw, D. M.; Robertson, S. H. *Variflex, 1.00*, 1999.

55.   Linstrom, P. J.; Mallard, W. G., Eds., NIST Chemistry WebBook, NIST Standard Reference Database Number 69, National Institute of Standards and Technology, Gaithersburg MD, 20899. http://webbook.nist.gov, (retrieved December 31, 2014): $\Delta_f H^o$(OH) = 8.9 kcal/mol, $\Delta_f H^o$ (CH$_3$C(O)F) = −105.7 kcal/mol, $\Delta_f H^o$(H$_2$O)= -57.8 kcal/mol, $\Delta_f H^o$ (CH$_2$CFO) = −59.0 kcal/mol.

56.   Feyereisen, M.; Feller, D.; Dixon, D., Hydrogen Bond Energy of the Water Dimer. *J. Phys. Chem.* **1996,** *100*, 2993-2997.

57.   Gonzalez-Lafont, A.; Lluch, J., Rate Constants of Gas-phase Hydrogen Abstraction Rreactions: a Balance between the Aassociation and the Abstraction Dynamical bottlenecks. *J. Molec. Struct.-Theochem* **2004,** *709*, 35-43.

58.   Johnston, H. S.; Heicklen, J., Tunnelling Corrections for Unsymmetrical Eckart Potential Energy Barriers. *J. Phys. Chem.* **1962,** *66*, 532-533.

59.   Ayala, P.; Schlegel, H., Identification and Treatment of Internal Rotation in Normal Mode Vibrational Analysis. *J. Chem. Phys.* **1998,** *108*, 2314-2325.

60.   Heard, D.; Pilling, M., Measurement of OH and HO2 in the Troposphere. *Chem. Rev.* **2003,** *103*, 5163-5198.

61.   George, C.; Saison, J.; Ponche, J.; Mirabel, P., Kinetics of Mass-transfer of Carbonyl Fluoride, Trifluoroacetyl Fluoride, and Trifluoroacetyl Chloride at the Air/Water Interface. *J. Phys. Chem.* **1994,** *98*, 10857-10862.

62.   De Bruyn, W.; Shorter, J.; Davidovits, P.; Worsnop, D.; Zahniser, M.; Kolb, C., Uptake of Haloacetyl and Carbonyl Halides by Water Surfaces. *Env. Sci. Technol.* **1995,** *29*, 1179-1185.

63.   Swain, G. C.; Scott, C. B., Rates of Solvolysis of Some Alkyl Fluorides and Chlorides. *J. Amer. Chem. Soc.* **1953,** *75*, 246-248.

64.   Bunton, C. A.; Fendler, J. H., The Hydrolysis of Acetyl Fluoride. *J. Org. Chem.* **1966,** *31*, 2301-2312.

65.   Kanakidou, M.; Dentener, F.; Crutzen, P., A global 3-dimensional Study of the Fate of HCFCs and HFC-134a in the Troposphere. *J. Geophys. Res. Atmos.* **1995,** *100* (D9), 18781-18801.

66.   Sander, R., Compilation of Henry's Law Constant for Inorganic and Organic Species of Potential Importance in Environmental Chemistry (Version 3). http://www.henrys-law.org, 1999.

Supporting Information

Experimental and Theoretical Study on the OH-reaction Kinetics and Photochemistry of Acetyl Fluoride (CH$_3$C(O)F) an Atmospheric Degradation Intermediate of HFC-161 (C$_2$H$_5$F)

Xinli Song,[1] Gábor L. Zügner,[2] Mária Farkas,[2] Ádám Illés,[2] Dariusz Sarzyński,[3] Tamás Rozgonyi,[2] Baoshan Wang*[1] and Sándor Dóbé*[2]

[1]College of Chemistry and Molecular Sciences, Wuhan University, Wuhan, 430072, People's Republic of China

[2]Institute of Materials and Environmental Chemistry, Research Centre for Natural Sciences, Hungarian Academy of Sciences, 1117 Budapest, Hungary

[3]Department of Physical Chemistry, Wroclaw Medical University, 50-556 Wroclaw, Poland

Song_SI_Argonne100_Revised

*Corresponding author. E-mail: baoshan@whu.edu.cn (B. Wang), dobe.sandor@ttk.mta.hu (S. Dóbé)
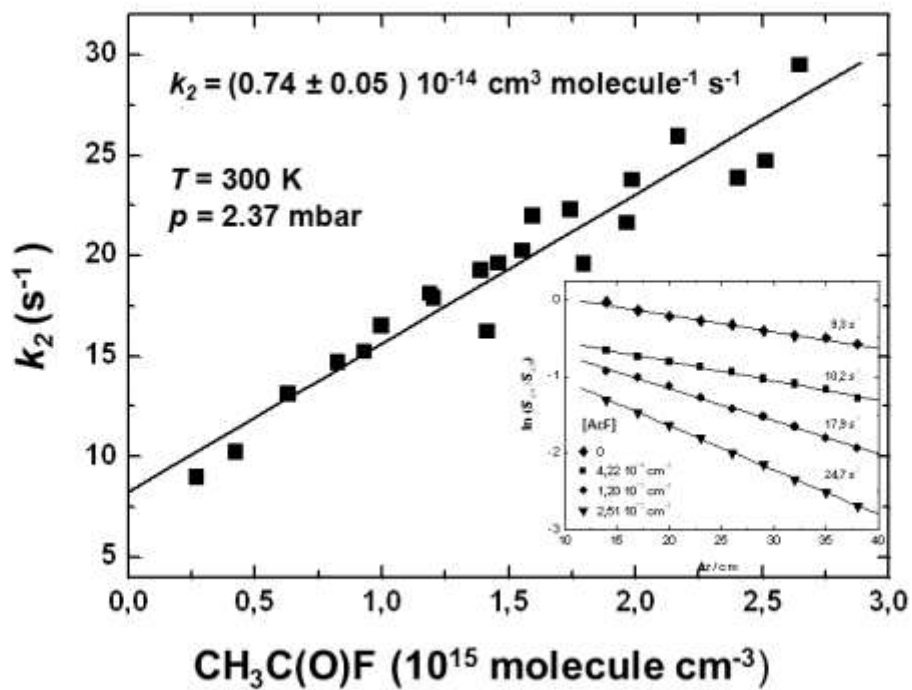
Figure SI-1. Pseudo-first order plots used for the determination of rate coefficient for the overall reaction of OH with CH$_3$(CO)F at $T = 300$ K and $p = 2.37$ mbar He pressure.
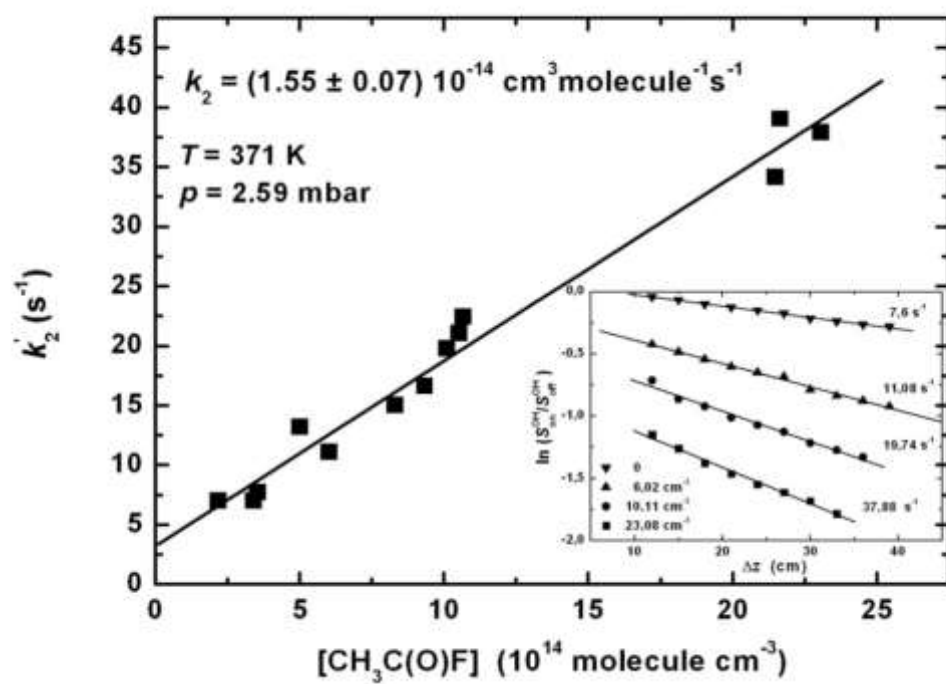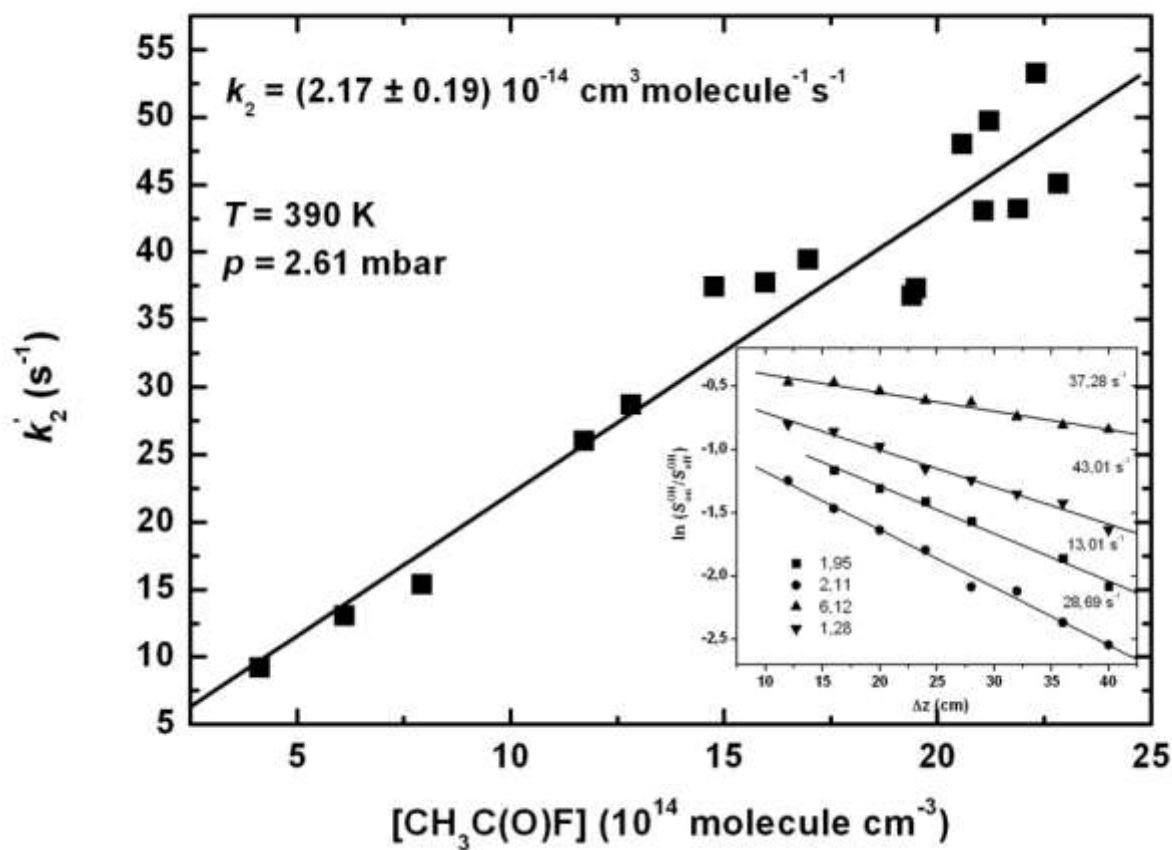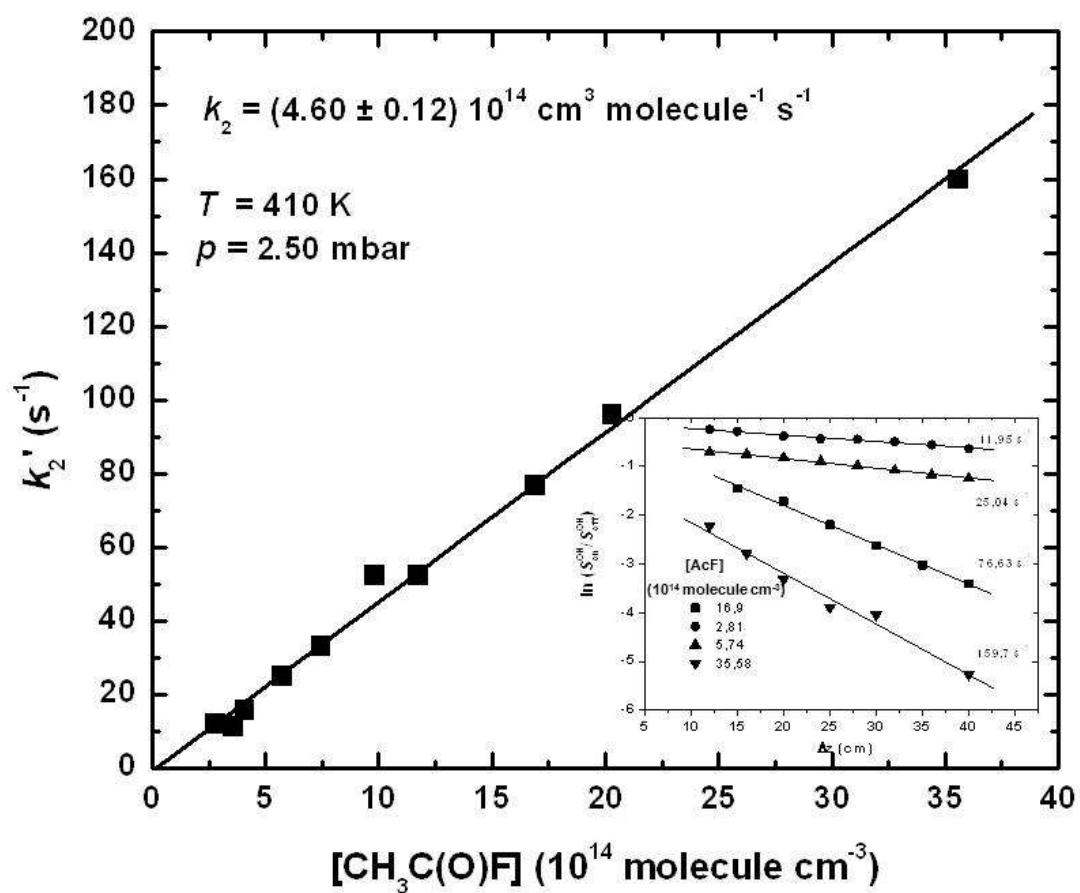
Figure SI-2. Pseudo-first order plots used for the determination of rate coefficient for the overall reaction of OH with CH$_3$(CO)F at $T = 371$ K and $p = 2.59$ mbar He pressure.

Figure SI-3. Pseudo-first order plots used for the determination of rate coefficient for the overall reaction of OH with CH$_3$(CO)F at $T = 390$ K and $p = 2.61$ mbar He pressure.
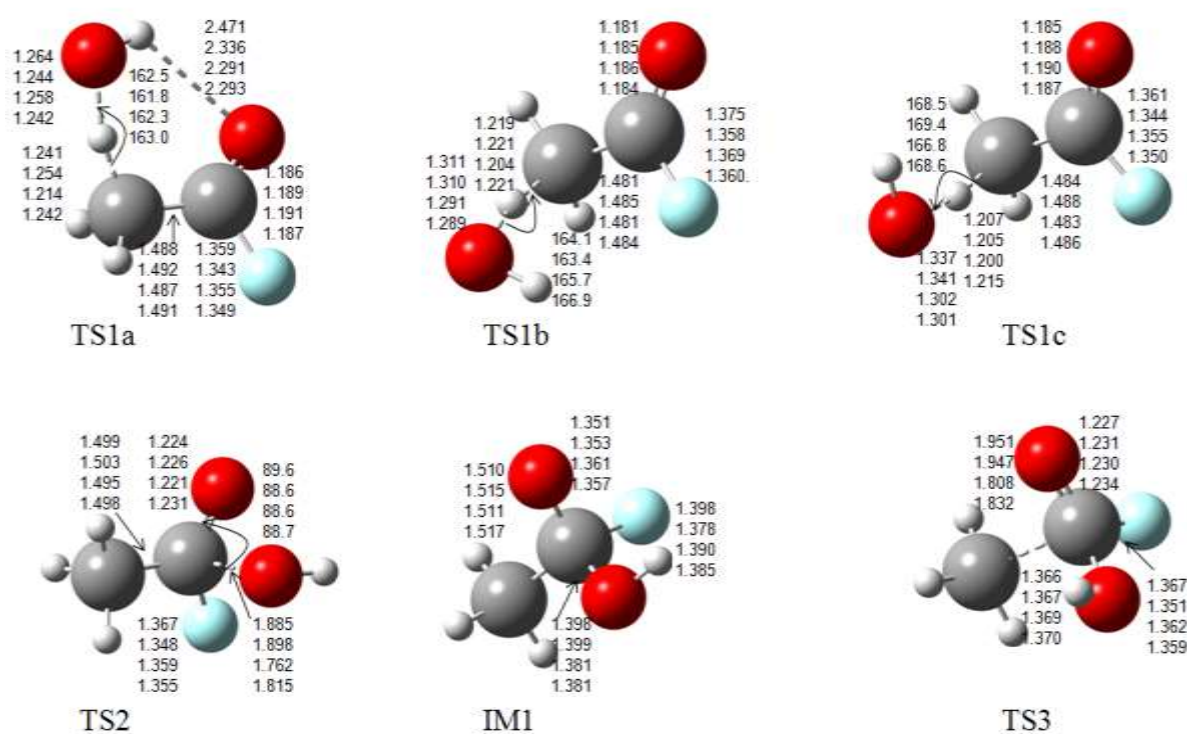
Figure SI-4. Pseudo-first order plots used for the determination of rate coefficient for the overall reaction of OH with $CH_3(CO)F$ at $T = 410$ K and $p = 2.50$ mbar He pressure.
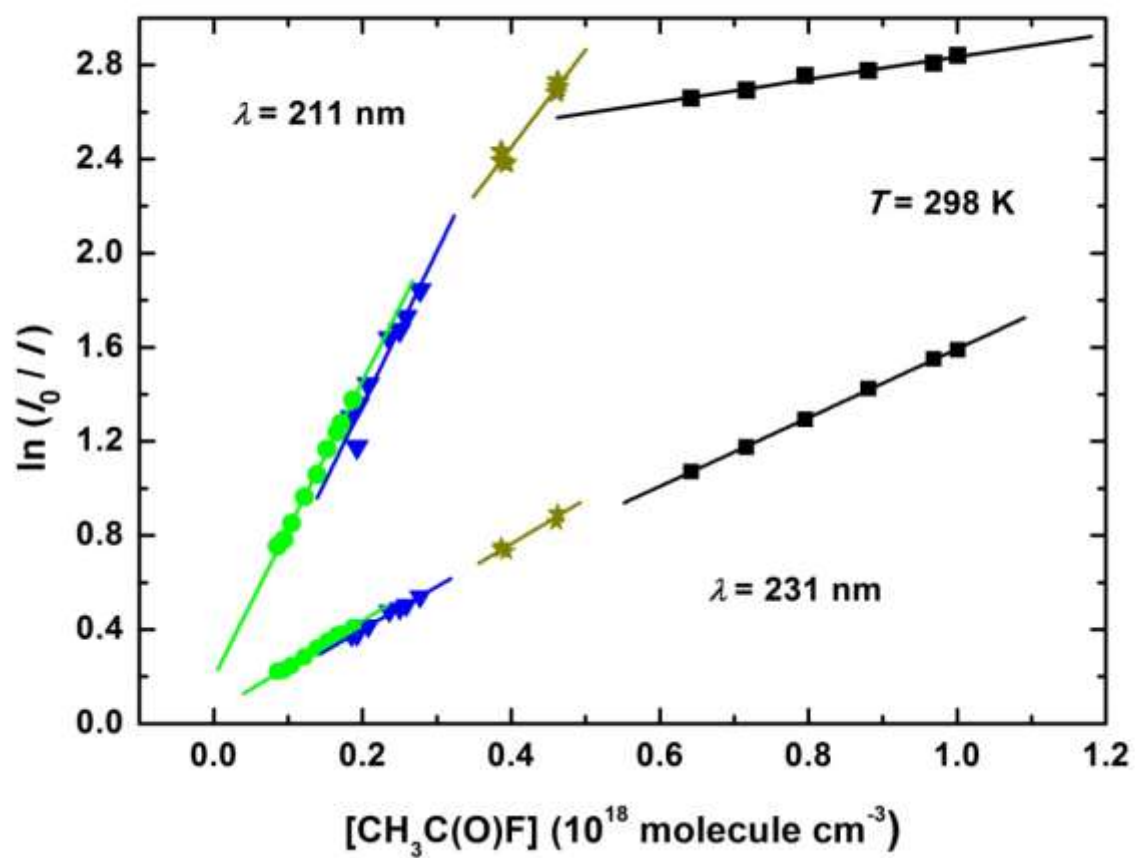
Figure SI-5. Selected Beer-Lambert plots for acetyl fluoride. Identical symbols indicate results that were obtained from the same series of experiments.

**Table SI-1.** Absorption cross sections of acetyl fluoride (base *e*) at T = 298 K (spectral resolution ~0.4 nm)

| λ (nm)	σ_{AcF} (10^{-20} cm^2 molecule^{-1})	$\pm 2\sigma$	λ (nm)	σ_{AcF} (10^{-20} cm^2 molecule^{-1})	$\pm 2\sigma$
201	11.311	0.157	232	3.535	0.047
202	11.771	0.128	233	3.250	0.031
203	12.058	0.125	234	2.897	0.036
204	12.366	0.087	235	2.678	0.053
205	12.577	0.139	236	2.326	0.037
206	12.842	0.075	237	2.081	0.033
207	12.886	0.069	238	1.691	0.040
208	12.926	0.101	239	1.410	0.051
209	12.914	0.088	240	1.107	0.038
210	12.814	0.106	241	0.854	0.050
211	12.543	0.074	242	0.651	0.036
212	12.276	0.124	243	0.546	0.053
213	12.121	0.130	244	0.454	0.049
214	11.688	0.151	245	0.370	0.056
215	11.337	0.138	246	0.300	0.053
216	10.862	0.185	247	0.270	0.054
217	10.508	0.183	248	0.193	0.052
218	10.087	0.185	249	0.168	0.057
219	9.572	0.184	250	0.164	0.047
220	8.991	0.173	251	0.120	0.056
221	8.512	0.159	252	0.091	0.056
222	7.973	0.092	253	0.078	0.043
223	7.541	0.127	254	0.067	0.043
224	6.934	0.050	255	0.056	0.046
225	6.407	0.019	256	0.048	0.050
226	5.937	0.043	257	0.044	0.046
227	5.465	0.042	258	0	-
228	5.037	0.036	259	0.008	0.038
229	4.612	0.039	260	0.005	0.038
230	4.151	0.041	>261	0	-
231	3.864	0.031			

Figure SI-6. Geometries of the key species involved in the OH + CH$_3$C(O)F reaction optimized at various levels of theory. From top to bottom: CBS-QB3, G4, MP2/aug-ccpVTZ, RCCSD(T)-F12/VDZ-F12. Distances are in Å and angles are in degrees.
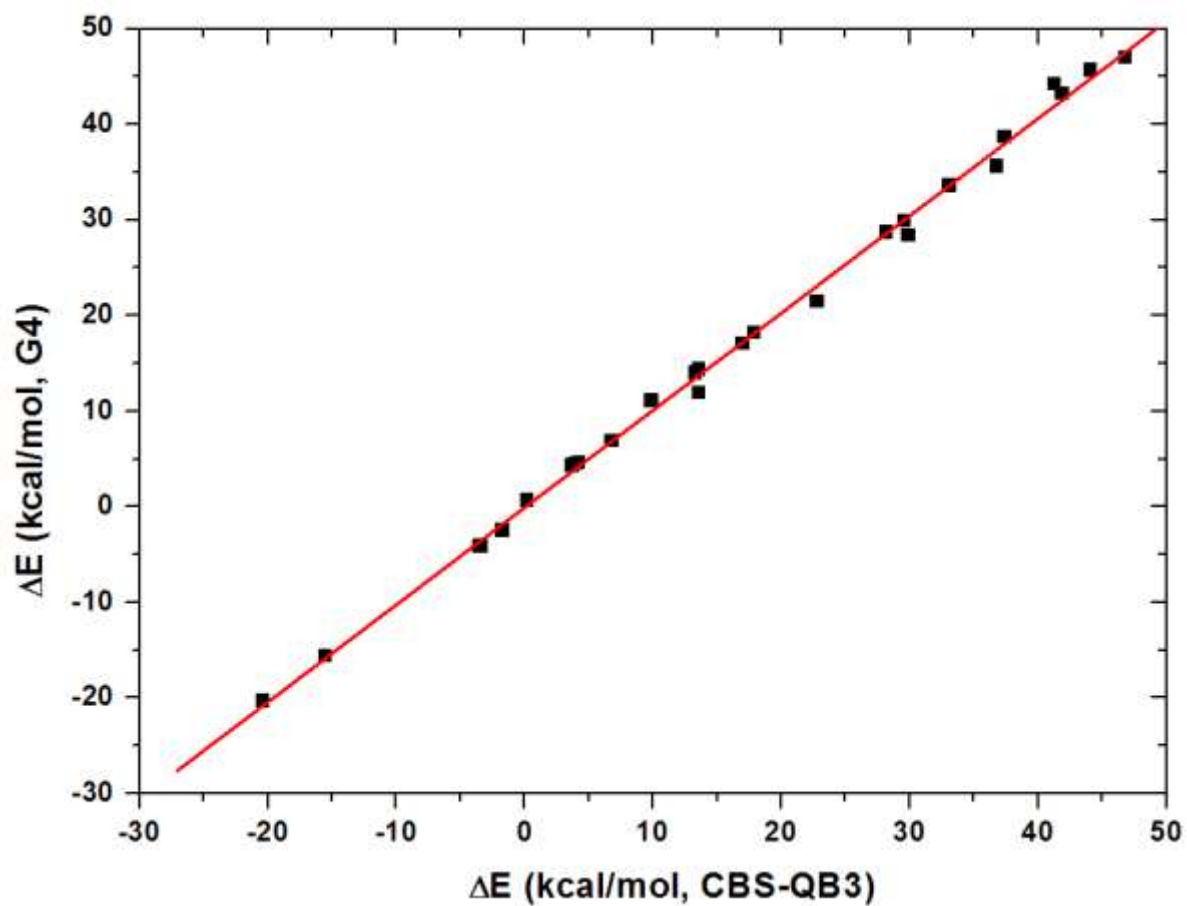
Figure SI-7. Correlation of all the relative energies involved in the OH+CH$_3$C(O)F reaction calculated at the CBS-QB3 and G4 levels of theory. The red line shows a linear fit to the scattered data with the expression: $\Delta E(G4) = 1.017 \times \Delta E(CBS\text{-}QB3) - 0.066$; $R^2 = 0.9987$.
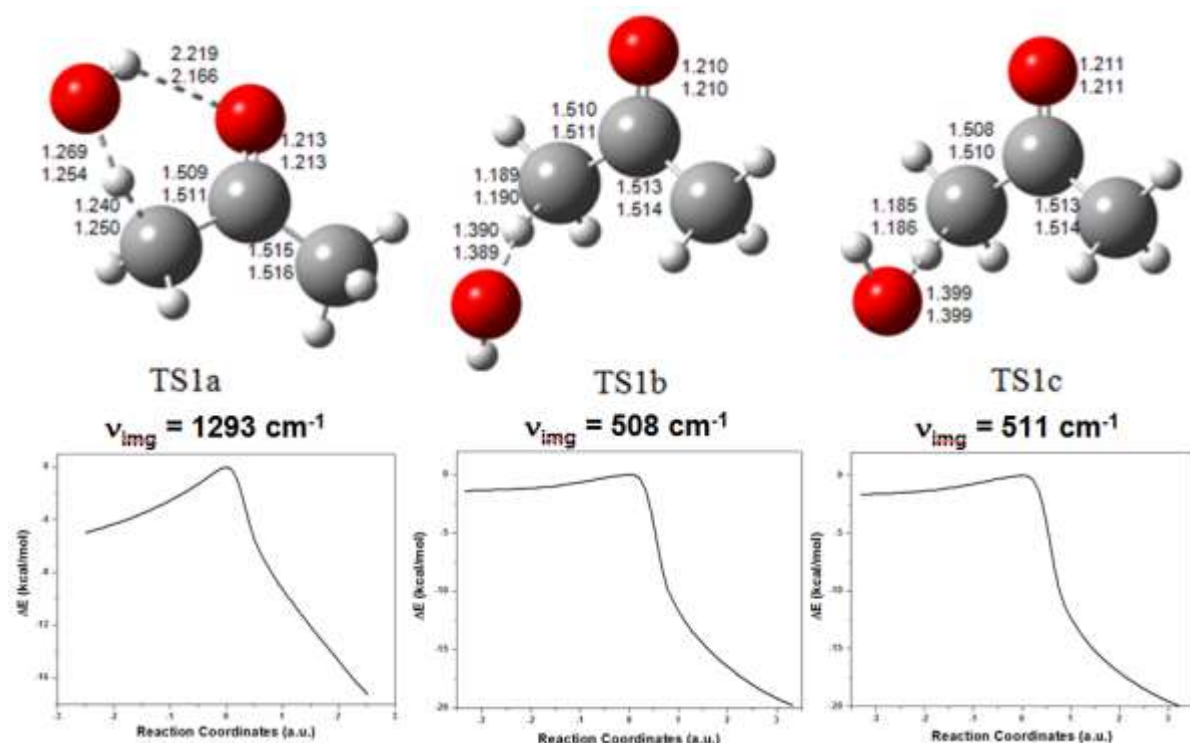
Figure SI-8. Geometries of the key species involved in the H-abstraction mechanism for the OH + CH$_3$C(O)CH$_3$ reaction optimized at the CBS-QB3 (upper cases) and G4 (lower cases) levels of theory, respectively. Distances are in Å and angles are in degrees. The CBS-QB3 calculated net barrier heights with respect to the OH + CH$_3$C(O)CH$_3$ asymptote for TS1a, TS1b, and TS1c are 1.4, 2.5, and 3.0 kcal/mol, respectively. The corresponding imaginary vibrational frequencies and the IRC profiles at the CBS-QB3 level are also shown.
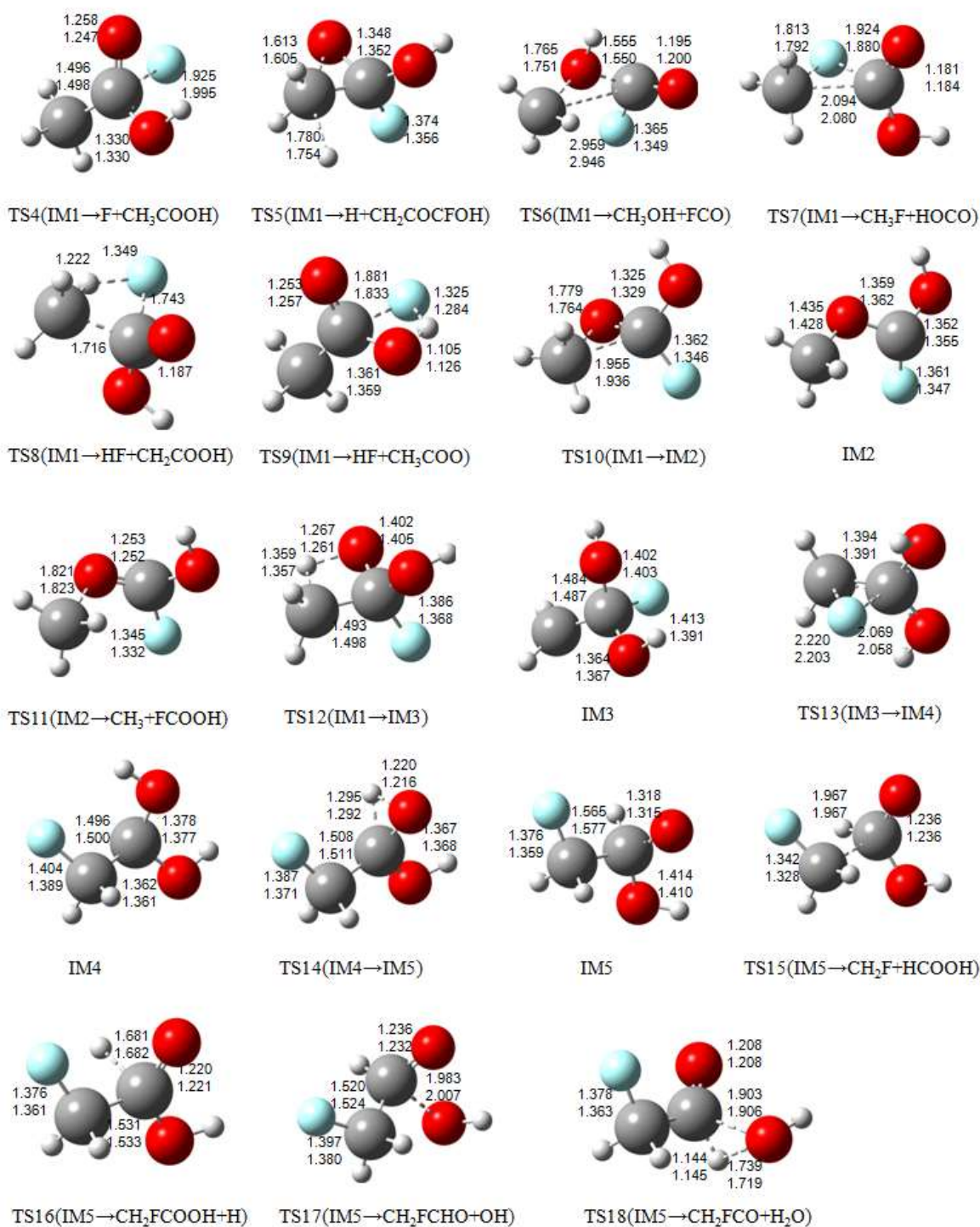
Figure SI-9. Geometries of the high-energy transition states and intermediates involved in the addition/elimination mechanism for the OH + CH₃C(O)F reaction optimized at the CBS-QB3 (upper cases) and G4 (lower cases) levels of theory, respectively. Distances are in Å and angles are in degrees.
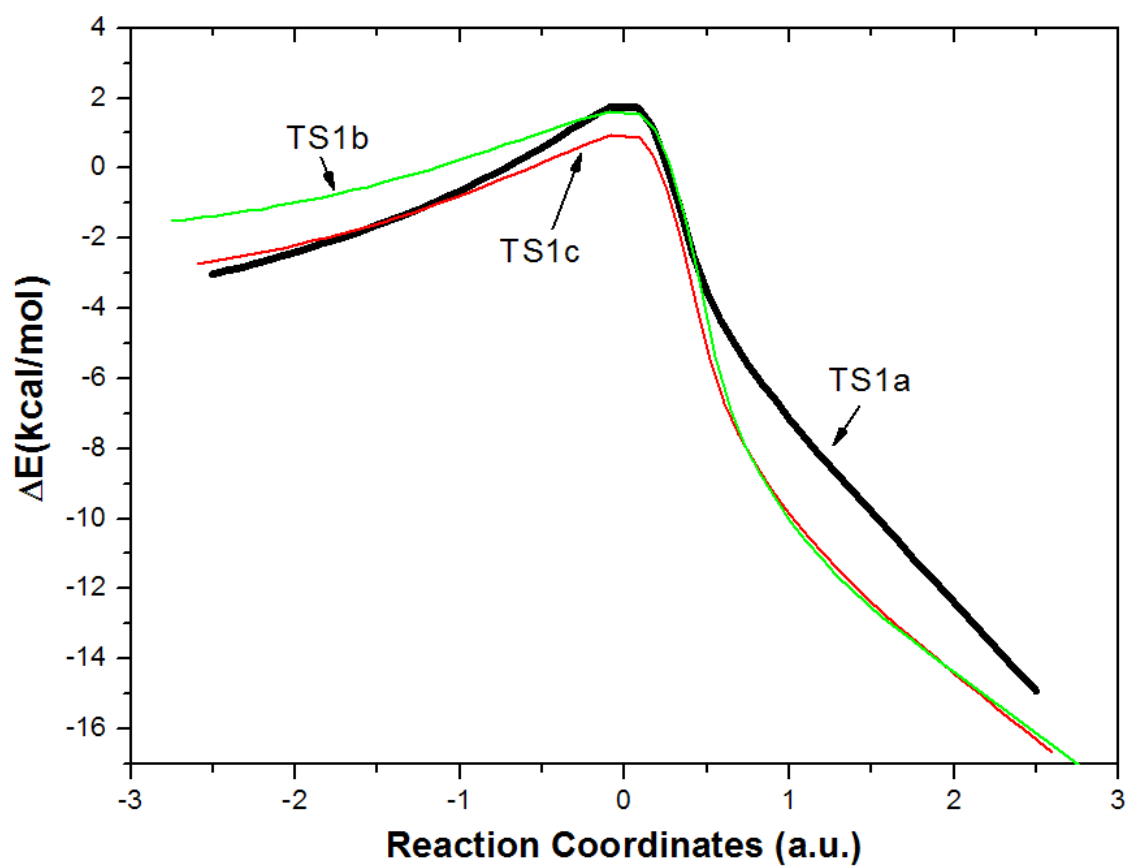
Figure SI-10. Profiles of the minimum energy reaction paths for the H-abstraction mechanism with respect to the OH + CH$_3$C(O)F reactants calculated at the CBS-QB3 level of theory (without zero-point energy corrections).